# Correlation between South China and India and development of double rift systems in the South China-India Duo during late Neoproterozoic time

Bingbing Liu[a,b,c], Touping Peng[a,b]*, Weiming Fan[c,d], Guochun Zhao[e], Jianfeng Gao[f], Xiaohan Dong[a,b,c], Shili Peng[a,b,c], Limin Wu[a,b,c], Bingxia Peng[a]

*a. State Key Laboratory of Isotope Geochemistry, Guangzhou Institute of Geochemistry, Chinese Academy of Sciences, Guangzhou 510640, China;*

*b. CAS Center for Excellence in Deep Earth Science, Guangzhou 510640, China*

*c. University of Chinese Academy of Sciences, Beijing 100049, China;*

*d. CAS Center for Excellence in Tibetan Plateau Earth Sciences, Beijing 100101, China;*

*e. Department of Earth Sciences, The University of Hong Kong, Hong Kong, China;*

*f. State Key Laboratory of Ore Deposit Geochemistry, Institute of Geochemistry, Chinese Academy of Sciences, Guiyang 550081, China*

*Corresponding author: Touping Peng

Address: Guangzhou Institute of Geochemistry,
Chinese Academy of Sciences,
P.O. Box 1131, Guangzhou 510640,
People's Republic of China
Fax: 86-20-85291510, Tel: 86-20-85290227

E-mail: tppeng08@126.com.

## Abstract

South China, India and their derivative terranes/blocks preserve a larger amount of similar magmatic and sedimentary records related to the tectonic transition from Rodinia to Gondwana. They provide crucial insights into not only the paleogeographic correlation between them but also the geodynamic mechanism for such a transition. Our new results together with published big data from these terranes/blocks point out that South China kept a linkage with India at least from the late Tonian (ca. 830 Ma) to Early Cambrian and formed the South China-India Duo located at the western margin of Rodinia. The identical magmatism and sedimentation reflect that double late Neoproterozoic rift systems in the South China-India Duo could have developed owing to the rollback of subducting oceanic slab beneath them, including an intracontinental rift (the Nanhua-Aravalli-Delhi rift) separating the Yangtze-Marwar from Cathaysia-Bundelkhand terranes and a contemporaneous intra-arc rift along the northern and western margins of the Yangtze Terrane, through the Marwar Terrane of western India, and then into the Seychelles and Madagascar terranes. Such an intra-arc rift is also the most feasible explanation for the common development of coeval arc-like and extension-related magmatic rocks and extensional sedimentary sequences on the western margin of the South China-India Duo and in Seychelles and Madagascar, and even other subduction zones.



**Key words:** Detrital zircon U-Pb-Hf isotope, Neoproterozoic-Early Paleozoic sedimentary sequences, South China-India Duo, late Neoproterozoic rift systems, Proto-Tethys Ocean

## 1. Introduction

Supercontinent forms when nearly all continental blocks on earth collide with each other and assemble into a solely large landmass (Zhao et al., 2018a). Rodinia and Gondwana are the most important ones of supercontinents in Earth's history (Zhao et al., 2018a). Increasing lines of evidence including reliable geological, paleomagnetic and paleontological data have established that they formed ca. 1.00 Ga and ca. 0.55 Ga ago, respectively (e.g., Cawood et al., 2013, 2018, and references therein). Although the paleogeographic position of major continental blocks in Rodinia and Gondwana have been widely accepted (Cawood et al., 2018; Zhao et al., 2018a), the reconstructions of some microcontinents in Rodinia and Gondwana and their tectonic evolution during the transition from Rodinia to Gondwana remain unknown. In particular, South China and India, as two important continental blocks in Asia, have been documented to be involved in the tectonic evolution of both Rodinia and Gondwana based on magmatic, sedimentary and paleontological evidence (e.g., Cawood et al., 2013, 2018; Jiang et al., 2003; Metcalfe, 2013; Yang et al., 2004; Zhao et al., 2018b). Their paleogeographic position and correlation in Rodinia and Gondwana and their tectonic affinity are still the subject of debate (Cawood et al., 2013, 2018; Chen et al., 2021; Jiang et al., 2003; Metcalfe, 2013; Wang et al., 2017a, 2021; Yang et al., 2004; Yao et al., 2014; Zhao et al., 2018b). Additionally, the tectonic framework and geodynamic mechanism for the tectonic evolution of supercontinents particularly during the transition from Rodinia to Gondwana remain unresolved (Cawood et al., 2018; Li et al., 2002; Wang et al., 2017a; Zhao et al.,

2018b). Fortunately, in recent years, a large number of data about Neoproterozoic-Early Paleozoic magmatic rocks and sedimentary sequences related to the tectonic evolution of these two landmasses in South China and India and even their derivative terranes/blocks have been published (Chen et al., 2021; Wang et al., 2017a, 2021; Yao et al., 2014; Zhao et al., 2018b). A combination and further analysis of these big data are crucial to decode the aforementioned issues.

In this contribution, we present new U-Pb and Lu-Hf isotopic analyses of detrital zircons of late Tonian to Ordovician sedimentary sequences from the Eastern Yidun subterrane of South China, and combined with other published big data from South China and other Gondwana- and Rodinia-derived continents, in order to re-evaluate the correlation between South China and India and decode their tectonic evolution during the transition from Rodinia to Gondwana. A new reconstruction model that South China was connected with India and formed the South China-India Duo during late Tonian-early Cambrian time is suggested. The breakup time of South China from Indian Gondwana after the Early Cambrian due to the opening of the Proto-Tethys Ocean is further constrained. Also, we propose the development of double late Neoproterozoic rift systems in the South China-India Duo, including an intra-arc rift along its western margin, and another intracontinental one (the Nanhua-Aravalli-Delhi rift) separating the Yangtze-Marwar from Cathaysia-Bundelkhand terranes in the interior of the South China-India Duo.

## 2. Geological background and samples

South China was formed by the amalgamation between the Yangtze Terrane to the northwest and the Cathaysia Terrane to the southeast along the Neoproterozoic Jiangnan fold belt (Cawood et al., 2018; Zhao et al., 2011). To its north is the North China Craton and to the southwest is the Indochina Block. It is bounded by the Yidun and Songpan-Ganzê terranes of the Tibetan Plateau to the northwest. The geological characteristics of the Yangtze and Cathaysia terranes have been summarized in detail by some authors (e.g., Cawood et al., 2013, 2018; Chen et al., 2021; Zhao et al., 2018b).

The Yidun Terrane is a microcontinent located between the Qiangtang and Songpan-Ganzê terranes, which is considered to be part of the Yangtze Terrane before the Mesozoic (BGMRSP, 1980, 1984). It is surrounded by two Paleo-Tethys suture zones, the Jinshajiang suture to the west and the Ganzê-Litang suture to the east (Fig. 1a, b; BGMRSP, 1984; Peng et al., 2014). To its southeast is the Yangtze Terrane, which is separated by the Longmenshan-Jinhe Fault (BGMRSP, 1984; Peng et al., 2014). Based on the tectono-stratigraphical distinction on the two flanks of the north-south-trending Xiangcheng-Geza Fault, the Yidun Terrane can be divided into the Western Yidun subterrane (also known as the Zhongza massif; Peng et al., 2014) and the Eastern Yidun subterrane (Fig. 1a, b; Peng et al., 2014).

The western subterrane consists mainly of greenschist to lower amphibolite facies Paleozoic meta-sedimentary rocks intercalated with minor meta-volcanics (BGMRSP, 1984). The eastern subterrane is dominated by Triassic volcano-clastic

111 rocks with minor Neoproterozoic-Paleozoic sedimentary successions in the southeast
112 (BGMRSP, 1984). The oldest strata are greenschist-amphibolite facies Neoproterozoic
113 Qiasi Group exposed in the southeast region of the Eastern Yidun subterrane,
114 comprising a suite of metamorphosed Neoproterozoic volcano-sedimentary
115 succession that consists of meta-volcanic, schist, leptynite and marble (Fig. 1;
116 BGMRSP, 1984). It can be divided into four segments from bottom to top based on its
117 lithologic association characteristics (Fig. 1c, d; BGMRSP, 1984). Unconformably
118 overlying the Qiasi Group is late Neoproterozoic (Ediacaran) sequences, comprised of
119 sandstone, carbonate and dolostone (BGMRSP, 1984). These strata are in turn
120 unconformably overlain by Early Cambrian carbonate intercalated with some
121 siliciclastics (BGMRSP, 1984). Ordovician succession, including sandstone, siltstone
122 and slate (Fig. 1 c, d; BGMRSP, 1984), unconformably overlies Lower Cambrian
123 strata, and is in turn unconformably overlain by Early Silurian slate and silicalite.
124 Above these strata are the Upper Paleozoic sedimentary rocks comprised of Devonian
125 schist, marble and sandstone, Carboniferous-Upper Permian limestone, Upper
126 Permian basalt and slate (BGMRSP, 1984). These Upper Paleozoic strata are
127 unconformably overlain by the Mesozoic and Paleogene sedimentary rocks in some
128 places (Fig. 1c; BGMRSP, 1984). In addition, voluminous Middle-Late Triassic
129 (230-206 Ma), and minor amount of Permian, Cretaceous and Cenozoic igneous rocks
130 are exposed in the Eastern Yidun subterrane (e.g., BGMRSP, 1984; Peng et al., 2014).

131 A total of five samples were collected for zircon U-Pb ages and Hf isotope
132 analyses (Table 1 and Figs. 1 & 2). Two schist samples (10YD-93 and 10YD-97) were

collected from the fourth and third segments of the Qiasi Group, respectively (Table 1 and Figs. 1 & 2). One sandstone sample (10YD-100) was collected from the Ediacaran Dengying Formation and a slate sample (10YD-102) and a schist sample (10YD-99) were collected from the Ordovician strata (Table 1 and Figs. 1 & 2).

## 3. Analytical methods

### *3.1 LA-ICP-MS zircon U-Pb dating*

ca. 5 kg of each sample was crushed and milled, and then zircons were separated using heavy-liquid and magnetic methods at the Laboratory of the Geological Team of Hebei Province, China. Cathodoluminescence (CL) images were taken at the Guangzhou Institute of Geochemistry, Chinese Academy of Sciences (GIG-CAS) for inspecting internal structures of individual zircons and for selecting positions for U-Pb and Lu-Hf isotope analyses. Detrital zircons of varying size and shape were selected randomly, leaving out grains with obvious cracks or inclusions.

In situ zircon U-Pb dating was carried out using an Agilent 7700x ICPMS coupled to a 193 nm ArF Excimer Laser ablation system (GeoLas 2005, Lambda Physik), housed at the Jupu analysis Lab, Nanjing of China. Analytical procedures were the same as those described by Liu et al. (2010). The frequency of laser system was 10 Hz. Gas flow rate of highly purified He as the carrier gas was 0.7 L/mn; auxiliary gas Ar was 1.13 L/mn. The spot diameter was 40 μm in size. Total acquisition time of one spot was 45 s. Zircon 91500 was used as external standard for

U-Pb dating, and was analyzed twice every 5 analyses. Time-dependent drifts of U-Th-Pb isotopic ratios were corrected using a linear interpolation (with time) for every five analyses according to the variations of 91500 (i.e., 2 zircon 91500 + 5 samples) (Liu et al., 2010). Preferred U-Th-Pb isotopic ratios used for 91500 are from Liu et al. (2010). Uncertainty of preferred values for the external standard 91500 was propagated to the ultimate results of the samples. Correction of common lead followed the method described by Liu et al. (2010). Data were processed with the ICPMSDataCal program (Liu et al., 2010). Uncertainties on individual analyses in data tables were reported at a 1σ level. Results were analyzed and plotted using Isoplot 3.0 (Ludwig, 2012). Zircon ages younger than 1000 Ma were based on $^{206}Pb/^{238}$ U ratios, and ages older than 1000 Ma were based on $^{207}Pb/^{206}Pb$ ratios. In this study, we excluded zircon age analyses with >10% discordance (Dickinson & Gehrels, 2009).

### *3.2 In-situ zircon Hf isotope analysis*

After the LA-ICP-MS zircon U-Pb dating, zircon Lu-Hf isotope compositions were analyzed by a 193 nm Ar-F excimer laser ablation system (RESOlution M-50-LR) attached to a multi-collector ICPMS (Neptune Plus), at GIG-CAS. The Hf isotopes were obtained with a beam diameter of 45 μm, pulse rate of 6 Hz, energy density of 80 J/cm$^2$ and Ablation time was 29 s. Quality control was made by measuring zircon standard Penglai for the unknown samples during the analyses to

evaluate the reliability of the analytical data, yielded weighted mean an average $^{176}Hf/^{177}Hf$ ratio of 0.282892 ± 0.000010 (1 standard deviation), which is consistent within errors with the reported values of 0.282906 ± 0.000010. In situ Hf isotope measurements were subsequently done on the same spots or the same age domains for age determinations of the concordant grains, as guided by CL images. The initial Hf isotopic ratios and crustal model ages were calculated using the dating results of the same spots.

## 4. Results

### *4.1 Zircon U-Pb geochronology*

The LA-ICP-MS U-Pb dating results of zircons for the studied samples are listed in Table S1. Most analyses were plotted on or near the concordia curve (Fig. 3). The detrital zircon U-Pb ages from the Eastern Yidun subterrane in this study show different age distribution patterns with unimodal detrital zircon pattern for the Neoproterozoic samples but multimodal pattern for the Ordovician ones (Fig. 3).

Zircon grains from all the Neoproterozoic samples in the Eastern Yidun subterrane are primarily euhedral and partly subeuhedral. All of them show magmatic oscillatory zoning in CL images (Fig. S1). 278 of 280 analyses produced 90-100% concordant ages, which were considered to be available for the following discussion. They gave an age spectrum ranging from 960 Ma to 574 Ma, and each sample displays a similar unimodal pattern with a single major age population at 800-760 Ma

196 (Table S1 and Fig. 3). Only one older age of ca. 960 Ma is present in the sample
197 10YD-97 (Table S1 and Fig. 3).

198 Most of zircon crystals from the Ordovician samples in the Eastern Yidun
199 subterrane are subeuhedral to subround while some grains are rounded. All the
200 analyzed zircon grains show magmatic oscillatory zoning in CL images (Fig. S1). 163
201 out of 165 analyses are less than 10% discordance, which are available for the
202 following discussion. The two Ordovician samples yielded U-Pb age varying from
203 3093 to 447 Ma. They share similar multimodal distribution patterns, with major age
204 populations at 600-500 Ma and 860-700 Ma and a subordinate age group at
205 2500-2400 Ma (Fig. 3). One difference is that the schist sample (10YD-99) has an
206 alternative Grenvillian age population at 1100-900 Ma (Fig. 3).

207 ***4.2 Zircon Hf isotopic compositions***

208 A total of 230 analyses for these three Neoproterozoic samples of the Eastern
209 Yidun subterrane exhibit a wide range of initial $^{176}Hf/^{177}Hf$ ratios from 0.282248 to
210 0.283031 (Table S2). Among them, 215 spots have positive $\varepsilon_{Hf}(t)$ values between +0.1
211 and +24.0 with $T_{DM}^{C}$ ages at 1.57-0.77 Ga (Table S2 and Fig.4), compatible with
212 those of the Neoproterozoic igneous rocks along the western and northern margins of
213 the Yangtze Terrane (Zhao et al., 2011). Only two Neoproterozoic zircons gave
214 slightly negative $\varepsilon_{Hf}(t)$ values of -2.1 and -1.2, respectively (Table S2 and Fig.4).

215 In the case of the Ordovician samples in the Eastern Yidun subterrane, a total of
216 75 analyses exhibit a wide range of initial $^{176}Hf/^{177}Hf$ ratios from 0.280824 to

0.282793, corresponding to large variations of $\varepsilon_{Hf}(t)$ values (-25.9 to +35.0), indicating a mixing products of the juvenile ($\varepsilon_{Hf}(t)>0$) and old ($\varepsilon_{Hf}(t)<0$) crustal rocks (Table S2 and Fig. 4). The main age group of 650-500 Ma have similar $\varepsilon_{Hf}(t)$ values (-25.0 to +6.1) with those of the magmatic rocks in the Kuunga Orogen (Zhu et al., 2011, and references therein), while the age cluster at 830-700 Ma yield similar $\varepsilon_{Hf}(t)$ values (-13.4 to +16.5) to those of the coeval igneous rocks in the Jiangnan Orogen in South China (Fig. 4; Yao et al., 2019). The 1100-900 Ma detrital zircons from the schist sample (10YD-99) show $\varepsilon_{Hf}(t)$ values ranging from -8.5 to +13.2, compatible with those in the Eastern Ghats Orogen and CITZ (Bhowmik et al., 2012; Zhu et al., 2011; and references therein). Minor ca. 2400 Ma zircons have variable $\varepsilon_{Hf}(t)$ values between -11.4 and +35.0.

## 5. Discussion

### *5.1. Sedimentary provenance*

By comparison, a unimodal age distribution pattern of the Neoproterozoic schists in the Eastern Yidun subterrane similar to those in the western Yangtze Terrane reflect a common provenance for the late Tonian-Ediacaran strata (Fig. 5). Owing to the absence of the Neoproterozoic moderate-felsic magmatic rocks within the Yidun Terrane (Tian et al., 2020), these Neoproterozoic detrital materials cannot be sourced from the interior of this terrane. In contrast, voluminous 0.86-0.70 Ga igneous rocks are exposed along the northern and western margins of the Yangtze Terrane, such as

238 the Neoproterozoic Panxi-Hannan arc (Zhao et al., 2018b; Zhou et al., 2006).
239 Moreover, the Hf isotopic compositions of detrital zircons from these Neoproterozoic
240 samples are in a good agreement with those of magmatic zircons of the
241 Neoproterozoic igneous rocks from the Panxi-Hannan arc (Fig. 4). In addition, these
242 detrital zircons of our Neoproterozoic samples are euhedral with magmatic zoning
243 (Fig. S1), indicating a short-distance transport from its provenance. Hence, we suggest
244 that the Neoproterozoic detritus in the Eastern Yidun subterrane could be mainly
245 sourced from the coeval igneous rocks in the Panxi-Hannan arc along the western and
246 northern margins of the Yangtze Terrane.

247 In the case of the Ordovician samples, they show a multimodal pattern
248 distinguishable from the unimodal one of the Neoproterozoic samples (Fig. 3). Except
249 for a similar major age of ca. 0.83-0.70 Ga to those Neoproterozoic samples, for
250 instance, they possess main age groups at ca. 0.65-0.50 Ga, ca. 1.00-0.90 Ga and a
251 subordinate age group at ca. 2.40 Ga (Fig. 3). Alternatively, the 0.83-0.70 Ga zircons
252 of the Ordovician samples have distinguishable $\varepsilon_{Hf}(t)$ values (-16.1 to +15.7) from
253 those of the Neoproterozoic samples (Table S2), but are similar to those of the coeval
254 igneous rocks in the Jiangnan Orogen in South China as mentioned before (Fig.4; Yao
255 et al., 2019). Taken together, it is obvious that the 0.83-0.70 Ga zircons of the
256 Ordovician samples could not originate mainly from the erosion of the Panxi-Hannan
257 arc magmatic rocks in the western Yangtze Terrane. In contrast, it is possible that most
258 of the 0.83-0.70 Ga zircons in the Ordovician sediments in the Eastern Yidun
259 subterrane were derived from the Jiangnan Orogen. Concerning the 1.00-0.90 Ga and

0.65-0.50 Ga detrital zircons, they were impossibly sourced from the coeval igneous rocks in the interior of South China due to the absence of synchronous magmatic rocks within South China. Therefore, they could be exotic by a long distance transport or recycled from the old strata in South China (Cawood et al., 2018), which are consistent with the subrounded and rounded attributes of these detrital zircons (Fig.S1). Indeed, the Ordovician sediments in the Eastern Yidun subterrane share a similar age spectrum and zircon Hf isotopic compositions to the Cambrian unit in the western Yangtze Terrane (Chen et al., 2021), indicating that the former could be primarily derived from the recycling of the latter, although their ultimate sources include the Eastern Ghats-Rayner Complex and the Kuunga Orogen located in the eastern India region, and the Jiangnan Orogen in South China.

### *5.2. Tectonic link between South China and India*

Two contrasting reconstruction models have been proposed for the paleogeographic position of South China in Rodinia: an internal location within the Rodinia supercontinent versus an external setting along the margin of the Rodinia supercontinent (e.g., Cawood et al., 2018; Li et al., 1999, and references therein; Zhao & Cawood, 1999). For the internal model, South China was located between the Laurentia and Australia blocks (e.g., Li et al., 1999; Li et al., 2002). In the peripheral model, South China was attached to India in the Early to Mid-Neoproterozoic (e.g., Cawood et al., 2018; Zhao et al., 2018b).

In fact, increasing lines of evidence including magmatic, paleomagnetic, and sedimentary data (e.g., Cawood et al., 2018; Chen et al., 2021; Gregory et al., 2009; Wang et al., 2017a, 2021; Yang et al., 2004; Yao et al., 2014; Zhao et al., 2018b), have demonstrated that South China could be located to the periphery of Rodinia rather than an intra-cratonic position during Neoproterozoic time. Nonetheless, the spatio-temporal evolution of South China within these peripheral models from Rodinia to Gondwana by different researchers is also different. For example, based on the paleomagnetic studies on the Middle Cambrian sediments from the western Yangtze Terrane, Yang et al. (2004) proposed that South China was connected with NW Australia during latest Proterozoic and Early Paleozoic times, until its breakup from Australia in the Middle Devonian. In contrast, by comparison of detrital zircon age spectra between the Gondwana-derived blocks/terranes, Yao et al. (2014) suggested that the Cathaysia side of South China was closely linked with the northern margin of India (the Himalaya region) by the Ediacaran-Cambrian collision between South China and India and persisted until the opening of the Paleo-Tethys Ocean during Devonian time. In recent years, by comparisons of magmatism, sedimentation, bio-stratigraphic affinity and paleomagnetic pole of South China with India and Australia, some researchers concluded that South China was most likely close to northern India during Neoproterozoic and even Early Cambrian times but was progressively separating from the latter, and rotating and migrating along the Gondwana margin toward northeastern India and NW Australia during latest Ediacaran or Early Cambrian time (e.g., Chen et al., 2021; Jiang et al., 2003; Wang et

al., 2021).

However, keeping a consistently main age group from the Tonian to Cambrian strata on the Cathaysia Terrane and on the western Yangtze Terrane although their main age groups are different, such as ca. 960 Ma for the former and ca. 800 Ma for the latter, respectively (Fig. 5; Wang et al., 2021; Yao et al., 2014), indicate that their detrital provenances did not change with time. In other words, they each shared a common source from the Tonian to Cambrian although the provenance is different between them. This, in turn, hints that the tectonic setting for the Tonian to Cambrian sedimentation in these two terranes did not change. Accordingly, it is unlikely that the Yangtze Terrane commenced to rift from northwestern India since the late Tonian and South China was migrating towards NW Australia. Moreover, the absence of diagnostic ca. 1170 Ma age group of NW Australia in the Tonian to Early Paleozoic strata in the Cathaysia Terrane (Fig. 5; e.g., Wang et al., 2010; Yao et al., 2014) also argues against a close proximity to NW Australia during Tonian to Early Paleozoic time. By contrast, the presence of a predominant age population of detrital zircons at ca. 960 Ma from the Tonian to Cambrian strata in the Cathaysia Terrane (Fig. 5; e.g., Wang et al., 2010; Yao et al., 2014), suggests that a common northern Indian (the Tethyan sequences) detrital provenance had continuously provided the detritus input into the Cathaysia Terrane from the Tonian to Cambrian. In fact, the similarities in facies assemblages of the late Neoproterozoic-Early Cambrian sedimentary rocks between South China and India also lend strong support to this proposition. For example, the Yangtze Terrane of South China and NW India share similar late Tonian

rift-related siliciclastic-volcanic successions, Cryogenian glaciogenic diamictite successions, Ediacaran carbonate successions, Early Cambrian phosphorite and clastic successions (Jiang et al., 2003). Correspondingly, the Cathaysia Terrane and eastern India region contain similar Tonian siliciclastics, Cryogenian sandstones and diamictites, Ediacaran-Cambrian siliciclastics (Wang & Li, 2003; Wang et al., 2021). As a consequence, we propose that South China should keep a close linkage with India and form the South China-India Duo at least during late Tonian to Cambrian time as the connection model proposed by Cawood et al. (2018) and Zhao et al. (2018b). It was finally separated from Indian Gondwana likely after the Early Cambrian due to the opening of Proto-Tethys Ocean (ca. 510 Ma) rather than Paleo-Tethys Ocean after the Devonian (also see discussion in Section 5.4).

### *5.3. Double late Neoproterozoic rift systems developed in the South China-India Duo*

Increasing lines of evidence, such as comparable Neoproterozoic rift-related magmatism and sedimentation between the Nanhua tectonic zone in South China and the Aravalli-Delhi fold belt in NW India, illustrate the development of a Neoproterozoic intracontinental linear rift basin in the interior of the South China-India Duo (Fig. 6; Wang & Li, 2003; Wang et al., 2017a; Zhao et al., 2018b, and references therein). For example, from a sedimentation perspective, some coeval extension-related basins with similar lithological assemblages and sedimentary sequences had developed in the Sindreth and Punagarh basins along the western

margin of the Aravalli-Dehli fold belt in NW India (Jiang et al., 2003; Zhao et al., 2018b, and references therein ), the unnamed basin in the Lesser Himalaya north of the Aravalli-Dehli fold belt (i.e., the Jaunsar-Simla and Blaini sequences; Jiang et al., 2003; Zhao et al., 2018b, and references therein), and the Nanhua basin in South China (Wang & Li, 2003; Zhao et al., 2018b). In addition, the late Tonian-Ediacaran sedimentary sequences in the Nanhua and Aravalli-Dehli basins share similar detrital zircon age patterns and overlapping $\varepsilon_{Hf}(t)$ values (Fig. 5), which also favors the idea of depositional continuity among the Nanhua-Aravalli-Dehli basin at that time. Besides, similar Neoproterozoic rift-related magmatism, including the bimodal magmatic rocks and A-type granites that are generally produced in extension-related regimes, has been identified in the Malani Igneous Suite located to the western margin of the NE-trending Aravalli-Dehli fold belt of NW India (e.g., Wang et al., 2017a; Zhao et al., 2018b; and references therein) and the Nanhua basin in South China (e.g., Deng et al., 2016; Li et al., 2021; Wang & Li, 2003). More importantly, the recognition of Late Neoproterozoic lower $\delta^{18}O$ magmatic zircons (<5‰) than that of mantle values (5.3 ± 0.6‰; Valley et al., 1998) in these two aforementioned belts (Fig. 6; Li et al., 2021; Wang et al., 2017a; Zhang et al., 2020a; Zhao et al., 2018b; and references therein), indicates the development of a synchronous rifting in NW India and the interior of South China as pointed out by Zhao et al. (2018b).

In fact, an alternative Neoproterozoic extension-related tectonic zone had also developed simultaneously along the northern and western margins of the Yangtze Terrane of South China. For instance, the occurrence of some Neoproterozoic

extension-related igneous rocks on the western margin of the Yangtze Terrane, including the Tiechuanshan (ca. 820 Ma) and Suxiong (ca. 800 Ma) bimodal volcanic rocks, and the Daxiangling (ca. 816 Ma), and Tiechuanshan, Huangguan and Mianning (780 Ma), and Panzhihua (750 Ma) A-type granites, and low-$\delta^{18}O$ magmatic rocks (Fig. 6; e.g., Li et al., 2002; Wu et al., 2020; and references therein), suggests an extensional setting at that time. Although a mantle plume setting has been invoked to account for such extension-related magmatism (Li et al., 2002; Wang et al., 2007a), this scenario fails to explain the presence of more voluminous 820-770 Ma magmatic rocks featured by typical arc geochemical signature in the Panxi-Hannan region on the northern and western Yangtze Terrane (Zhao et al., 2011; Zhao et al., 2018b; and references therein). In contrast, a prolonged subduction-related arc environment as proposed by some authors (Cawood et al., 2018; Zhao et al., 2018b; Zhou et al., 2006; and references therein) can have also developed at 820-770 Ma. Moreover, the arc-like geochemical characteristics and high proportion of younger detrital zircon age population (CA-DA<100 Ma in 30% of the zircon population; Fig. 7) of the Neoproterozoic metasedimentary samples from the Yidun Terrane also indicated the deposition in a convergent setting basin (Cawood et al., 2012; Tian et al., 2020). In this respect, a back-arc environment is likely a plausible interpretation for the coexistence of arc- and extension-type magmatic rocks on the western and northern margins of the Yangtze Terrane, as assumed recently by Luo et al. (2018). However, such a model is incompatible with their magmatic pattern dominated by arc-type magmatic rocks with some extension-related rocks in this region as

391 mentioned before (Cawood et al., 2018; Zhao et al., 2018b). In other words, these
392 Neoproterozoic arc-type magmatic rocks should represent the important component of
393 simultaneous continental arc. Moreover, considering that a huge thickness of
394 extension-related late Neoproterozoic volcaniclastic sediments (> 5 km) coexist with
395 synchronous magmatic rocks on the northern and western margins of the Yangtze
396 Terrane and the southeastern margin of the Ganzê and Yidun terranes (BGMRSP,
397 1984), we propose that an intra-arc rifting is the most feasible explanation for such a
398 coupling of magmatism and sedimentation. In fact, intra-arc rifting has been
399 established in different subduction zones, such as northeast Japan of west Pacific
400 (Nakajima, 2013), and the Anglona region of northwestern Sardinia, Italy (Sowerbutts,
401 2000). In particular, the magmatic association and sedimentary pattern on the northern
402 and western margins of the Yangtze Terrane are similar to those in the intra-arc rift
403 basin in the Anglona region of northwestern Sardinia, Italy (Sowerbutts, 2000).

404 As the important parts of the Neoproterozoic subduction system on the western
405 margin of Rodinia (e.g., Cawood et al., 2018; Wang et al., 2021; Zhao et al., 2018b),
406 the coexistence of coeval extension-related magmatic rocks and sedimentary basins
407 together with a large number of subduction-related arc-type igneous rocks in
408 Madagascar and Seychelles likewise indicates the development of an intra-arc rifting
409 at that time, resembling those on the western and northern margins of the Yangtze
410 Terrane as stated above. For instance, the recognition of some mafic-ultramafic
411 plutons with layered Fe-Ti-V oxide mineralization, A-type granitoids with a strongly
412 alkaline composition and bimodal magmatic suite in the Imorona-Itsindro Suite of

central Madagascar (Archibald et al., 2017; Nédélec et al., 2016; Zhou et al., 2018a; and references therein), coupled with the same extensional structural signature between the ca. 790 Ma Imorona-Itsindro rocks and their country rocks (Nédélec et al., 2016, and references therein), has been recently interpreted as the products of continental rifting by Zhou et al. (2018a). Furthermore, from a variation of isotopic composition perspective, especially for zircon Hf and O isotopes of the 850-750 Ma magmatic rocks in the central Madagascar, Zhou et al. (2018a) believed that synchronous continental rifting had been involved in their petrogenesis. On the other hand, these central Madagascar rocks are dominated by calc-alkaline series and geochemically show an affinity to volcanic or continental arc magmatic rocks, most researchers ascribed their generation to the results of prolonged Andean-like arc magmatism (Archibald et al., 2017; Handke et al., 1999; Kröner et al. 2000; Tucker et al. 1999b). In Seychelles, the 810-700 Ma magmatic rocks also display the coupling of a typical Andean-type arc and rift-type (low-$\delta^{18}O$ granites) geochemical signatures (e.g., Ashwal et al., 2002, and references therein). Taken together, we propose that a late Neoproterozoic intra-arc rift system could have developed along the northern and western margins of the Yangtze Terrane, through the Marwar Terrane of western India, and then into Seychelles and Madagascar, although such lines of evidence from western India are still absent so far (Fig. 6). Such an intra-arc rift system along the western margin of the South China-India Duo is different from the contemporaneous intracontinental one (the Nanhua-Aravalli-Delhi rift system) within it (Fig. 6). Moreover, it can also account for the contradiction about the common presence of

435 coeval arc-type and extension-related magmatic rocks coupled with some
436 extension-related sedimentation in the same area.

437 The most plausible mechanism responsible for the development of such double
438 synchronous rift systems should be attributed to the rollback of subducting oceanic
439 slab beneath the South China-India Duo (Fig. 6), which would result in the
440 asthenospheric upwelling and subsequent lithospheric extension at that time. As the
441 old suture belts, the Jiangnan fold belt between the Yangtze and Cathaysia terranes in
442 South China (Zhao et al., 2011) and the Aravalli-Dehli fold belt between the Marwar
443 and Bundelkhand terranes in NW India (Zhao et al., 2018b) are the most ideal areas to
444 produce lithospheric extension. As a result, it is the most effective mechanism to
445 induce an intracontinental rifting. An alternative region apt to trigger lithospheric
446 extension is the continental arc, especially the intra-arc where arc magmatism
447 develops frequently and trans-lithospheric faults widely occur. Such a scenario can
448 also be an important mechanism for the fragmentation of some
449 micro-continents/terranes/blocks from a big continent by the intra-arc rifting.

450

451 ***5.4. Implication for breakup of South China from Gondwana***

452 Different researchers have proposed different breakup times for South China from
453 Gondwana. For example, earlier studies suggested the separating time from the Early
454 Cambrian to Silurian in light of the variation of biogeography and stratigraphy in
455 South China (Jiang et al., 2003, and references therein). Subsequently, considering the

456 opening of Paleo-Tethys Ocean between the South China and Indochina blocks, most
457 workers believed that South China had broken up from Gondwana in the Devonian
458 (e.g., Cawood et al., 2013; Chen et al., 2021; Metcalfe, 2013; Wang et al., 2021). The
459 critical evidence is the dating results of the remnant oceanic components, the oldest
460 plagiogranites of which at Shuanggou from the Jinshajiang-Ailaoshan Paleo-Tethys
461 suture yielded zircon U-Pb ages of ca. 383-376 Ma (Jian et al., 2009). More recently,
462 by comparison of the Neoproterozoic to Early Paleozoic detrital zircon age spectra of
463 South China with India and Australia, Wang et al. (2021) and Chen et al. (2021)
464 proposed the initial separation time of South China from NW India in the Cryogenian
465 and Early Cambrian, respectively. Moreover, based on the opening of Paleo-Tethys
466 Ocean, they both concluded that South China should have finally drifted away from
467 the northern margin of Australian Gondwana in the Devonian (Chen et al., 2021;
468 Wang et al., 2021).

469 Regardless of how South China broke up from Gondwana, all the views ignore a
470 crucial fact that the Proto-Tethys Ocean between South China and other
471 Gondwana-derived blocks had also developed in the Early Paleozoic. The opening of
472 the Proto-Tethys Ocean should have ever led to the separation of South China from
473 northern Gondwana. For instance, the Early Paleozoic oceanic relics, including
474 477-460 Ma MORB-type clinopyroxenite, gabbro and amphibolite, and 519-502 Ma
475 plagiogranites in the Tam Ky-Phuoc Son suture of Vietnam (Gardner et al., 2017;
476 Nguyen et al., 2019, and references therein), indicate the presence of an Early
477 Paleozoic Ocean between the South China and Indochina blocks or South

China-northern Indochina and southern Indochina blocks (Faure et al., 2018; Nguyen et al., 2019). On the other hand, another Proto-Tethys Ocean (518-438 Ma) between the South Qiangtang-Baoshan and North Qiangtang-Indochina terranes has been also documented in recent years (e.g., Hu et al., 2014; Wu, 2013). In particular, the identification of the Cambrian ophiolites (ca. 517-490 Ma; Hu et al., 2014; Wu, 2013) implies the development of a Tethys Ocean at least in the Middle Cambrian. In this regard, it is suggested that the Indochina Block had rifted away from the northern margin of Gondwana in the Middle Cambrian-Early Silurian interval. It is, in turn, the most plausible to infer that South China had been ever separated from the northern Gondwana at least from the Middle Cambrian to Early Silurian (Fig. 8; Liu et al., 2020a).

Whether South China had been assembled together with northern Gondwana by continent-continent collision similar to the collision between the South China and Indochina blocks in the Late Silurian remains unknown. Although Zhang et al. (2014) proposed a continent-continent collision time at 427-422 Ma based on the study of high-pressure basic granulites in the Central Qiangtang of Tibet, the identification of coeval (438±11 Ma) oceanic cumulate gabbro in the same ophiolitic complex belt of central Qiangtang likely indicates that the Early Paleozoic Proto-Tethys Ocean had not been closed (Wu, 2013). In fact, no age-equivalent collision-related records have been discovered so far in the Changning-Menglian ophiolite belt that represents the southern continuation of the central Qiangtang Proto-Tethys Ocean. More importantly, the identification of the Early and Late Paleozoic oceanic OIB-type mafic rocks that

had commonly experienced a same Late Triassic ultrahigh-pressure metamorphism (Fan et al., 2015), indicates that the Proto-Tethys Ocean could have developed persistently from the Early Paleozoic to the end of the Paleozoic (Liu et al., 2020a, and references therein). Therefore, it is most likely that the Central Qiangtang high-pressure granulites within Tibet (Zhang et al., 2014) could be the products of Early Paleozoic arc-continent collision during the tectonic evolution of a single Proto- and Paleo-Tethys Ocean. Combing with all data (Chen et al., 2021, and references therein), we propose that the South China and Indochina blocks were separated from Indian Gondwana after the Early Cambrian and were not welded with Gondwana again, although they were likely amalgamated together during Late Silurian time (Faure et al., 2018; Nguyen et al., 2019) until the opening of the Paleo-Tethys Ocean between them (Jian et al., 2009).

## 6. Conclusions

Our new zircon U-Pb dating and Hf isotope analysis for the Neoproterozoic-Early Paleozoic (meta-) sedimentary sequences from the Eastern Yidun subterrane that belongs to part of the Yangtze Terrane of South China, coupled with a detailed compilation of big data published from South China, India and some blocks/terranes separated from them, can draw the following conclusions:

(1) The Neoproterozoic sediments in the Eastern Yidun subterrane were sourced mainly from the Panxi-Hannan magmatic arc on the northern and western margins of

the Yangtze Terrane while the Ordovician sequences were recycled from the Cambrian strata in the western Yangtze Terrane.

(2) South China kept a connection with India and formed the South China-India Duo located at northwestern margin of Rodinia during late Tonian (ca. 800 Ma) to Early Cambrian time.

(3) Double late Neoproterozoic rift systems had developed in the South China-India Duo owing to the rollback of subducting oceanic slab beneath it, including an intra-arc rift along the northern and western margins of the Yangtze Terrane, through the Marwar Terrane of western India, and then into the Seychelles and Madagascar, and another coeval intracontinental one (the Nanhua-Aravalli-Delhi rift) separating the Yangtze-Marwar from Cathaysia-Bundelkhand terranes within the interior of the South China-India Duo.

(4) South China was finally separated from northern India during Middle Cambrian-Ordovician time due to the opening of the Proto-Tethys Ocean (ca. 510 Ma) but was not welded with Gondwana again.

## Acknowledgements

This work was jointly supported by the National Second Expedition to the Tibetan Plateau (2019QZKK0702) and National Natural Science Foundation of China (92055207, 42072263, 41490613, 41672058). This is a contribution from the Guangzhou Institute of Geochemistry, Chinese Academy of Sciences (GIG, CAS; No. xxx). All data of this manuscript will be available at the Mendelay Data repository (DOI: 10.17632/bs75p9fx6h.1).

# References


Ao, W. H., Zhao, Y., Zhang, Y. K., Zhai, M. G., Zhang, H., Zhang, R. Y., Wang, Q., & Sun, Y., 2019. The neoproterozoic magmatism in the northern margin of the yangtze block: insights from Neoproterozoic (950-706 Ma) gabbroic-granitoid rocks of the Hannan complex. *Precambrian Research*, 333, 105442. DOI: 10.1016/j.precamres.2019.105442

Armistead, S. E., Collins, A. S., Merdith, A. S., Payne, J. L., Cox, G. M., Foden, J. D., Razakamanana, T., De Waele, B., 2019. Evolving Marginal Terranes During Neoproterozoic Supercontinent Reorganization: Constraints From the Bemarivo Domain in Northern Madagascar. *Tectonics*, 38(6), 2019-2035. DOI: 10.1029/2018TC005384

Ashwal, L. D., Demaiffe, D., Torsvik, T. H., 2002. Petrogenesis of Neoproterozoic granitoids and related rocks from the Seychelles: the case for an Andean-type arc origin. *Journal of Petrology*, 43(1), 45-83. DOI: 10.1093/petrology/43.1.45

Bureau of Geology and Mineral Resources of Sichuan Province (BGMRSP), 1980. *The Geological map of the People's Republic of China, Yidun Regional (scale 1: 200,000)*. (Map H-47-16). Sichuan: BGMRSP. (in Chinese)

Bureau of Geology and Mineral Resources of Sichuan Province (BGMRSP), 1984. *The Geological map of the People's Republic of China, Gongling Regional (scale 1: 200,000)*. (Map H-47-35). Sichuan: BGMRSP. (in Chinese)

Cawood, P. A. & Buchan, C., 2007. Linking accretionary orogenesis with supercontinent assembly. *Earth Science Reviews*, 82(3-4), 217-256. DOI: 10.1016/j.earscirev.2007.03.003

Cawood, P. A., Hawkesworth, C., Dhuime, B., 2012. Detrital zircon record and tectonic setting. *Geology*, 40, 875-878. DOI: 10.1130/G32945.1

Cawood, P. A., Wang, Y. J., Xu, Y. J., Zhao, G. C., 2013. Locating South China in Rodinia and Gondwana: a fragment of greater India lithosphere? *Geology*, 41 (8), 903-906. DOI: 10.1130/G34395.1

Cawood, P. A., Zhao, G. C., Yao, J. L., Wang, W., Xu, Y. J., Wang, Y. J., 2018.

573 Reconstructing South China in Phanerozoic and Precambrian supercontinents.
574 *Earth Science Reviews*, 186, 173-194. DOI: 10.1016/j.earscirev.2017.06.001
575 Chen, Q., Sun, M., Long, X., Zhao, G., & Yuan, C., 2016. U-Pb ages and Hf isotopic
576 record of zircons from the late Neoproterozoic and Silurian-Devonian sedimentary
577 rocks of the western Yangtze block: implications for its tectonic evolution and
578 continental affinity. *Gondwana Research*, 184-199. DOI: 10.1016/j.gr.2015.01.009
579 Chen, Q., Sun, M., Long, X., Zhao, G., Wang, J., Yu, Y., & Yuan, C., 2018.
580 Provenance study for the Paleozoic sedimentary rocks from the west Yangtze Block:
581 constraint on possible link of South China to the Gondwana supercontinent
582 reconstruction. *Precambrian Research*, 309, 271-289.
583 https://doi.org/10.1016/j.precamres.2017.01.022
584 Chen, Q., Zhao, G., Sun, M., 2021. Protracted northward drifting of South China
585 during the assembly of Gondwana: Constraints from the spatial-temporal
586 provenance comparison of Neoproterozoic-Cambrian strata. *Geological Society of*
587 *America Bulletin*, 1-17. https://doi.org/10.1130/B35791.1
588 Cui, X., Zhu, W. B., Fitzsimons, I. C. W., He, J. W., Lu, Y. Z., Wang, X., Ge, R. F.,
589 Zheng, B. H. & Wu, X., 2015. U-Pb age and Hf isotope composition of detrital
590 zircons from Neoproterozoic sedimentary units in southern Anhui Province, South
591 China: implications for the provenance, tectonic evolution and glacial history of the
592 eastern Jiangnan Orogen. *Precambrian Research*, 271, 65-82.
593 https://doi.org/10.1016/j.precamres.2015.10.004
594 DeCelles, P. G., Gehrels, G. E., Quade, J., Lareau, B. & Spurlin, M., 2000. Tectonic
595 implications of U-Pb zircon ages of the Himalayan orogenic belt in Nepal. *Science*,
596 288(5465), 497-499. DOI: 10.1126/science.288.5465.497
597 Deng, Q., Wang, Z., Jian, W., Hu, Z., Fei, Y., 2016. 800~780 Ma continental rift
598 magmatism in the eastern part of the Jiangnan orogen: implications from ~790 Ma
599 aluminous A-type granites in Zhejiang-Anhui-Jiangxi border area. *Geological*
600 *Bulletin of China*, 35(11), 1855-1868.
601 Dickinson, W. R., Gehrels, G. E., 2009. Use of U-Pb ages of detrital zircons to infer
602 maximum depositional ages of strata: a test against a Colorado Plateau Mesozoic

603 database. *Earth and Planetary Science Letters*, 288(1-2), 115-125.
604 https://doi.org/10.1016/j.epsl.2009.09.013
605 Fan, W. M., Wang, Y. J., Zhang, Y. H., Zhang, Y. Z., Jourdan, F., & Liu, H.C., 2015.
606 Paleotethyan subduction process revealed from Triassic blueschists in the Lancang
607 tectonic belt of Southwest China. *Tectonophysics*, 662, 95-108.
608 https://doi.org/10.1016/j.tecto.2014.12.021
609 Faure, M., Nguyen, V.V., Hoai, L.T.T., Lepvrier, C., 2018. Early Paleozoic or
610 Early-Middle Triassic collision between the South China and Indochina Blocks: the
611 controversy resolved? Structural insights from the Kon Tum massif (Central
612 Vietnam). *Journal of Asian Earth Sciences*, 166, 162-180.
613 https://doi.org/10.1016/j.jseaes.2018.07.015.
614 Gardner, C. J., Graham, I. T., Belousova, E., Booth, G. W., & Greig, A., 2017.
615 Evidence for Ordovician subduction-related magmatism in the Truong Son terrane,
616 SE Laos: implications for Gondwana evolution and porphyry Cu exploration
617 potential in SE Asia. *Gondwana Research*, 44, 139-156.
618 DOI:10.1016/j.gr.2016.11.003
619 Gehrels, G. E., Decelles, P. G., Ojha, T. P., & Upreti, B. N., 2006. Geologic and U-Pb
620 geochronologic evidence for early paleozoic tectonism in the Dadeldhura thrust
621 sheet, far-west Nepal Himalaya. *Journal of Asian Earth Sciences*, 28(4-6), 385-408.
622 https://doi.org/10.1016/j.jseaes.2005.09.012
623 Gehrels, G., Kapp, P., Decelles, P., Pullen, A., Blakey, R., Weislogel, A., et al., 2011.
624 Detrital zircon geochronology of pre-tertiary strata in the Tibetan-Himalayan
625 orogen. *Tectonics*, 30(5), 1-27. https://doi.org/10.1029/2011TC002868
626 Gregory, L. C., Meert, J. G., Bingen, B., Pandit, M. K., & Torsvik, T. H., 2009.
627 Paleomagnetism and geochronology of the Mlani igneous suite, northwest India:
628 implications for the configuration of Rodinia and the assembly of Gondwana.
629 *Precambrian Research*, 170(1-2), 13-26. DOI: 10.1016/j.precamres.2008.11.004
630 Haines, P. W., Kirkland, C. L., Wingate, M. T. D., Allen, H., Belousova, E. A., &
631 Gréau, Y., 2016. Tracking sediment dispersal during orogenesis: A zircon age and
632 Hf isotope study from the western Amadeus Basin, Australia. *Gondwana Research*,

633 37, 324-347. https://doi.org/10.1016/j.gr.2015.08.011
634 Handke, M. J., Tucker, R. D., & Ashwal, L. D., 1999. Neoproterozoic continental arc
635 magmatism in west-central Madagascar. *Geology*, 27(4), 351-354.
636 https://doi.org/10.1130/0091-7613(1999)027<0351:NCAMIW>2.3.CO;2
637 Harris, C., & Ashwal, L. D., 2002. The origin of low delta O-18 granites and related
638 rocks from the Seychelles. *Contributions to Mineralogy and Petrology*, 143(3),
639 366-376. DOI: 10.1007/s00410-002-0349-6
640 He, Y. Y., Niu, Z. J., Yao, H. Z., Song, F., & Yang, W. Q., 2020. Provenance and
641 tectonic setting of the Ordovician sedimentary succession at the southeastern
642 margin of the Yangtze Block, South China: Implications for paleotopographic
643 evolution of northestern Gondwana. *Journal of Asian Earth Sciences*, 202,
644 104532.https://doi.org/10.1016/j.jseaes.2020.104532
645 Hofmann, M. H., Li, X. H., Chen, J., MacKenzie, L. A., & Hinman, N. W., 2016.
646 Provenance and temporal constraints of the early Cambrian Maotianshan shale,
647 Yunnan province, China. *Gondwana Research*, 37, 348-361. DOI:
648 10.1016/j.gr.2015.08.015
649 Hofmann, M., Linnemann, U., Rai, V., Becker, S., Gartner, A. & Sagawe, A., 2011.
650 The India and South China cratons at the margin of Rodinia-synchronous
651 Neoproterozoic magmatism revealed by LA-ICP-MS zircon analyses. *Lithos*,
652 123(1-4), 176-187. https://doi.org/10.1016/j.lithos.2011.01.012
653 Hu, P. Y., Li, C., Wu, Y. W., Xie, C. M., Wang, M., Zhang, H. Y., & Li, J., 2014. The
654 Silurian Tethyan Ocean in central Qiangtang, northern Tibet: Constraints from
655 zircon U-Pb ages of plagiogranites within the Taoxinghu ophiolite. *Geological*
656 *Bulletin of China*, 33(11), 1651-1661.
657 Huang, D. L., Wang, X. L., Xia, X. P., Wan, Y. S., Zhang, F. F., Li, J. Y., & Du, D. H.,
658 2018. Neoproterozoic Low-delta O-18 Zircons Revisited: Implications for Rodinia
659 Configuration. *Geophysical Research Letters*, 46(2), 678-688. DOI:
660 10.1029/2018GL081117
661 Hughes, N. C., Myrow, P. M., Ghazi, S., McKenzie, N. R., Stockli, D. F., DiPietro, J.
662 A., 2019. Cambrian geology of the Salt Range of Pakistan: Linking the Himalayan

663 margin to the Indian craton. *Geological Society of America Bulletin*, 131(7-8),
664 1095-1114. DOI: 10.1130/B35092.1
665 Hughes, N. C., Myrow, P. M., McKenzie, N. R., Harper, D. A. T., Bhargava, O. N.,
666 Tangri, S. K., Ghalley, K. S., and Fanning, C. M., 2011. Cambrian rocks and faunas
667 of the Wachi La, Black Mountains, Bhutan. *Geological Magazine*, 148(3), 351-379.
668 DOI: 10.1017/S0016756810000750
669 Jian, P., Liu, D. Y., Kr?ner, A., Zhang, Q., Wang, Y. Z., Sun, X. M., & Zhang, W.,
670 2009. Devonian to Permian plate tectonic cycle of the Paleo-Tethys Orogen in
671 southwest China: Insights from zircon ages of ophiolites, arc/back-arc assemblages
672 and within-plate igneous rocks and generation of the Emeishan CFB province.
673 *Lithos*, 113: 767-784. https://doi.org/10.1016/j.lithos.2009.04.006
674 Jiang, G. Q., Sohl, L. E., & Christie-Blick, N., 2003. Neoproterozoic stratigraphic
675 comparison of the Lesser Himalaya (India) and Yangtze block (South China):
676 Paleogeographic implications. *Geology*, 31(10), 917-920. DOI: 10.1130/G19790.1
677 Jiang, X. W., Zou, H., Bagas, L., Chen, H. F., Liu, H., Li, Y., Li, M., & Li, D., 2020.
678 The Mojiawan I-type granite of the Kangding Complex in the western Yangtze
679 Block: new constraint on the Neoproterozoic magmatism and tectonic evolution of
680 South China. *International Geology Review*, 1-21. DOI:
681 10.1080/00206814.2020.1833254
682 Johnson, E. L., Phillips, G., & Allen, C. M., 2016. Ediacaran-Cambrian basin
683 evolution in the Koonenberry Belt (eastern Australia): implications for the
684 geodynamics of the Delamerian Orogen. *Gondwana Research*, 37, 266-284. DOI:
685 10.1016/j.gr.2016.04.010
686 Keemana, J., Turnera, S., Haines, W. P., Belousova, E., Ireland, T., Brouwer, P., Foden,
687 J., & W?rner, G., 2020. New U-Pb, Hf and O isotope constraints on the provenance
688 of sediments from the Adelaide Rift Complex-Documenting the key
689 Neoproterozoic to early Cambrian succession. *Gondwana Research*, 83, 248-278.
690 https://doi.org/10.1016/j.gr.2020.02.005
691 Kröener, A., Hegner, E., Collins, A. S., Windley, B. F., Brewer, T. S., Razakamanana,
692 T., & Pidgeon, R. T., 2000. Age and magmatic history of the Antananarivo Block,

693 central Madagascar, as derived from zircon geochronology and Nd isotopic
694 systematics. *American Journal of Science*, 300(4), 251-288. DOI:
695 https://doi.org/10.2475/ajs.300.4.251
696 Lan, Z. W., Zhang, S. J., Li, X. H., Pandey, S. K., Sharma, M., Shukla, Y., Ahmad, S.,
697 Sarkar, S. & Zhai, M. G., 2020. Towards resolving the 'jigsaw puzzle' and
698 age-fossil inconsistency within East Gondwana. *Precambrian Research*, 345, 1-18.
699 https://doi.org/10.1016/j.precamres.2020.105775
700 Li, J. Y., Wang, X. L., & Gu, Z. D., 2018. Petrogenesis of the Jiaoziding granitoids
701 and associated basaltic porphyries: Implications for extensive early Neoproterozoic
702 arc magmatism in western Yangtze Block. *Lithos*, 296, 547-562. DOI:
703 10.1016/j.lithos.2017.11.034
704 Li, X. H., Li, W. X., Li, Z. X., & Liu, Y., 2008. 850-790 Ma bimodal volcanic and
705 intrusive rocks in northern Zhejiang, South China: a major episode of continental
706 rift magmatism during the breakup of Rodinia. *Lithos*, 102(1-2), 341-357. DOI:
707 10.1016/j.lithos.2007.04.007
708 Li, X. H., Li, Z. X., Zhou, H. W., Liu, Y., & Kinny, P. D., 2002. U-Pb zircon
709 geochronology, geochemistry and Nd isotopic study of Neoproterozoic bimodal
710 volcanic rocks in the Kangdian Rift of South China: Implications for the initial
711 rifting of Rodinia. *Precambrian Research*, 113 (1-2), 135-154. DOI:
712 10.1016/S0301-9268(01)00207-8
713 Li, Y. X., Yin, C. Q., Lin, S. F., Zhang, J., Gao, P., Qian, J. H., Xia, Y. F. & Liu, J. N.,
714 2021. Geochronology and geochemistry of bimodal volcanic rocks from the
715 western Jiangnan Orogenic Belt: Petrogenesis, source nature and tectonic
716 implication. *Precambrian Research*, 359, 106218.
717 https://doi.org/10.1016/j.precamres.2021.106218
718 Li, Z. X., Li, X. H., Kinny, P. D., & Wang, J., 1999. The breakup of Rodinia: did it
719 start with a mantle plume beneath South China? *Earth and Planetary Science*
720 *Letters*, 173(3), 171-181. https://doi.org/10.1016/S0012-821X(99)00240-X
721 Liu, B. B., Peng, T. P., Fan, W. M., Zhao, G. C., Gao, J. F., Dong, X. H., & Peng, B.
722 X., 2020. Tectonic Evolution and Paleoposition of the Baoshan and Lincang Blocks

of West Yunnan During the Paleozoic. *Tectonics*, 39(10), e2019TC006028.

Liu, H., Wang, Z. J., Deng, Q., Du, Q. D., & Yang, F., 2019a. Constraints on the onset age of the Sturtian glaciation from the Southeast Yangtze Block, South China. International *Geology Review*, 61(15), 1876-1886. https://doi.org/10.1080/00206814.2019.1566787

Liu, S. L., Cui, X. Z., Wang, C. L., Ren, G. M., Wang, P., Pang, W. H., & Ren, F., 2020. New Sedimentological and Geochronological Evidence for Mid-Neoproterozoic Rifting in Western Yangtze Block, South China. *Earth Science*, 45(8), 3082-3093 (In Chinese with English abstract). DOI: 10.3799/dqkx.2020.145

Liu, X. J., Xu, Z. Q., Zhen, Y. L. and Ma, Z. L., 2019c. Characteristics of detrital zircon U-Pb geochronology and Hf isotopics from Liwu Group within the Changqiang dome on the southeastern margin of Songpan-Ganzi terrane and its tectonic implications. *Acta Petrologica Sinica*, 35(6): 169-1716. (In Chinese with English abstract). DOI: 10.18654/1000-0569 /2019. 06. 05

Liu, Y. S., Hu, Z. C., Zong, K. Q., Gao, C. G., Gao, S., Xu, J., & Chen, H. H., 2010. Reappraisement and refinement of zircon U-Pb isotope and trace element analyses by LA-ICP-MS. *Chinese Science Bulletin*, 55(15), 1535-1546. DOI: 10.1007/s1143-010-3052-4

Liu, Y., Yang, K. G., Polat, A., & Ma, X., 2019b. Reconstruction of the Cryogenian palaeogeography in the Yangtze Domain: constraints from detrital age patterns. *Geological Magazine*, 56(7), 1247-1264. DOI: 10.1017/S0016756818000535

Long, S., Mcquarrie, N., Tobgay, T., Rose, C., Gehrels, G., & Grujic, D., 2011. Tectonostratigraphy of the lesser Himalaya of Bhutan: implications for the along-strike stratigraphic continuity of the northern Indian margin. *Geological Society of America Bulletin*, 123(7-8), 1406-1426. DOI: 10.1130/B30202.1

Ludwig, K. R., 2003. User's manual for Isoplot 3.00: A geochronological toolkit for Microsoft Excel. Berkeley Calif: Berkeley Geochronology Center.

Luo, B. J., Liu, R., Zhang, H. F., Zhao, J. H., Yang, H., Xu, W. C., Guo, L., Zhang, L. Q., Tao, L., Pan, F. B., Wang, W., Gao, Z. & Shao, H., 2018. Neoproterozoic continental back-arc rift development in the Northwestern Yangtze Block: Evidence

753 from the Hannan intrusive magmatism. *Gondwana Research*, 59, 27-42. DOI:
754 10.1016/j.gr.2018.03.012
755 Luo, L., Zeng, L. B., Wang, K., Yu, X.X., Li, Y.H., Zhu, C.X. & Liu, S. N., 2020.
756 Provenance investigation for the Cambrian-Ordovician strata from the northern
757 margin of the western Yangtze Block: implications for locating the South China
758 Block in Gondwana. *Geological Magazine*, 157(4), 551-572.
759 https://doi.org/10.1017/S0016756819001110
760 Ma, X., Yang, K. G., & Polat, A., 2019. U-Pb ages and Hf isotopes of detrital zircons
761 from pre-Devonian sequences along the southeast Yangtze: a link to the final
762 assembly of East Gondwana. *Geological Magazine*, 156(6), 950-968. DOI:
763 10.1017/S0016756818000511
764 Malone S. J., Meert, J. G., Banerjee, D. M., Pandit, M. K., Tamrat, E., Kamenov, G.
765 D., Pradhan, V. R. & Sohl, L. E., 2008. Paleomagnetism and detrital zircon
766 geochronology of the upper Vindhyan Sequence, Son Valley and Rajasthan, India:
767 A ca. 1000 Ma Closure age for the Purana Basins. *Precambrian Research*, 164(3-4),
768 137-159. https://doi.org/10.1016/j.precamres.2008.04.004
769 Mckenzie, N. R., Hughes, N. C., Myrow, P. M., Xiao, S., & Sharma, M., 2011.
770 Correlation of Precambrian-Cambrian sedimentary successions across northern
771 India and the utility of isotopic signatures of Himalayan lithotectonic zones. *Earth
772 and Planetary Science Letters*, 312(3-4), 471-483. DOI: 10.1016/j.epsl.2011.10.027
773 McKenzie, N.C., Hughes, P. M., Myrow, P. M., Banerjee, D. M., Deb, M., &
774 Planavsky N. J., 2013. New age constraints for the Proterozoic Aravalli-Delhi
775 successions of India and their implications. *Precambrian Research*, 238, 120-128.
776 https://doi.org/10.1016/j.precamres.2013.10.006
777 Mcquarrie, N., Long, S. P., Tobgay, T., Nesbit, J. N., Gehrels, G., & Ducea, M. N.,
778 2013. Documenting basin scale, geometry and provenance through detrital
779 geochemical data: lessons from the Neoproterozoic to Ordovician lesser, greater,
780 and Tethyan Himalayan strata of Bhutan. *Gondwana Research*, 23(4), 1491-1510.
781 https://doi.org/10.1016/j.gr.2012.09.002
782 Metcalfe, I., 2013. Gondwana dispersion and Asian accretion: Tectonic and

783 palaeogeographic evolution of eastern Tethys. *Journal of Asian Earth Sciences*, 66,
784 1-33. https://doi.org/10.1016/j.jseaes.2012.12.020
785 Mukherjee, P. K., Jain, A. K., Singhal, S., Singha, N. B., Singh, S., Kumud, K., Seth,
786 P. & Patel, R. C., 2019. U-Pb zircon ages and Sm-Nd isotopic characteristics of the
787 lesser and great Himalayan sequences, Uttarakhand Himalaya, and their regional
788 tectonic implications. *Gondwana Research*, 75, 282-297.
789 https://doi.org/10.1016/j.gr.2019.06.001
790 Mulder, J. A., Everard, J. L., Cumming, G., Meffre, S., Bottrill, R. S., Merdith, A. S.,
791 Halpine, J. A., McNeill, A. W., & Cawood, P. A., 2020. Neoproterozoic opening of
792 the Pacific Ocean recorded by multi-stage rifting in Tasmania, Australia. *Earth*
793 *Science Reviews*, 201, 1-29. https://doi.org/10.1016/j.earscirev.2019.103041
794 Myrow, P. M., Hughes, N. C., Goodge, J. W., Fanning, C. M., Williams, I. S., & Peng,
795 S., 2010. Extraordinary transport and mixing of sediment across Himalayan central
796 Gondwana during the Cambrian-Ordovician. *Geological Society of America*
797 *Bulletin*, 122(9-10), 1660-1670. https://doi.org/10.1130/B30123.1
798 Nédélec, A., Paquette, J. L., Antonio, P., Paris, G., & Bouchez, J. L., 2016. A-type
799 stratoid granites of Madagascar revisited: Age, source and links with the breakup of
800 Rodinia. *Precambrian Research*, 280, 231-248.
801 https://doi.org/10.1016/j.precamres.2016.04.013
802 Nguyen, Q. M., Feng, Q., Zi, J. W., Zhao, T., Tran, H. T., Ngo, T. X., Tran, D. M. &
803 Nguyen, H. Q., 2019. Cambrian intra-oceanic arc trondhjemite and tonalite in the
804 Tam Ky-Phuoc Son Suture Zone, central Vietnam: Implications for the early
805 Paleozoic assembly of the Indochina Block. *Gondwana Research*, 70,
806 151-170.https://doi.org/10.1016/j.gr.2019.01.002
807 Peng, T. P., Zhao, G. C., Fan, W. M., Peng, B. X., & Mao, Y. S., 2014. Zircon
808 geochronology and Hf isotopes of Mesozoic intrusive rocks from the Yidun terrane,
809 Eastern Tibetan Plateau: petrogenesis and their bearings with Cu mineralization.
810 *Journal of Asian Earth Sciences*, 80, 18-33. DOI: 10.1016/j.jseaes.2013.10.028
811 Qasim, M., Ding, L., Khan, M. A., Umar, M., Jadoon, I. A. K., Haneef, M., Baral, U.,
812 Cai, F. L., Shah, A. & Yao, W., 2018. Late Neoproterozoic-early Palaeozoic

stratigraphic succession, western Himalaya, North Pakistan: detrital zircon provenance and tectonic implications. *Geological Journal*, 53(9), 2258-2279. DOI: 10.1002/gj.3063

Qi, H., & Zhao, J. H., 2020b. Petrogenesis of the neoproterozoic low-δ18O granitoids at the western margin of the Yangtze block in South China. *Precambrian Research*, 351, 105953. https://doi.org/10.1016/j.precamres.2020.105953

Qi, L., Cawood, P. A., Xu, Y. J., Du, Y. S., Zhang, H. C. & Zhang, Z. K., 2020a. Linking south china to north India from the late Tonian to Ediacaran: constraints from the Cathaysia block. *Precambrian Research*, 350, 105898. https://doi.org/10.1016/j.precamres.2020.105898

Qi, L., Xu. Y. J., Cawood, P. A., & Du, Y. S., 2018. Reconstructing Cryogenian to Ediacaran successions and paleogeography of the South China Block. *Precambrian Research*, 314, 452-467. https://doi.org/10.1016/j.precamres.2018.07.003

Shellnutt, J. G., Nguyen, D. T., & Lee, H. Y., 2020. Resolving the origin of the Seychelles microcontinent: Insight from zircon geochronology and Hf isotopes. *Precambrian Research*, 343, 105725. DOI: 10.1016/j.precamres.2020.105725

Sowerbutts, A., 2000. Sedimentation and volcanism linked to multiphase rifting in an Oligo-Miocene intra-arc basin, Anglona, Sardinia. *Geological Magazine*, 137(4), 395-418. https://doi.org/10.1017/S0016756800004246

Sun, J. J., Shu, L. S., Santosh, M., & Wang, L. S., 2018. Precambrian crustal evolution of the central Jiangnan Orogen (South China): Evidence from detrital zircon U-Pb ages and Hf isotopic compositions of Neoproterozoic metasedimentary rocks. *Precambrian Research*, 318, 1-24. DOI: 10.1016/j.precamres.2018.09.008

Sun, W. H., Zhou, M. F., Gao, J. F., Yang, Y. H., Zhao, X. F. & Zhao, J. H., 2009. Detrital zircon U-Pb geochronological and Lu-Hf isotopic constraints on the precambrian magmatic and crustal evolution of the western Yangtze block, SW China. *Precambrian Research*, 172(1-2), 99-126. DOI: 10.1016/j.precamres.2009.03.010

Sun, W. H., Zhou, M. F., Yan, D. P., Li, J. W. & Ma, Y. X., 2008b. Provenance and tectonic setting of the Neoproterozoic Yanbian group, western Yangtze block (SW

China). *Precambrian Research*, 167(1), 213-236. https://doi.org/10.1016/j.precamres.2008.08.001

Tian, Z. D., Leng, C. B., & Zhang, X. C., 2020. Provenance and tectonic setting of the neoproterozoic meta-sedimentary rocks at southeastern Tibetan plateau: implications for the tectonic affinity of Yidun terrane. *Precambrian Research*, 344, 1-19. https://doi.org/10.1016/j.precamres.2020.105736

Turner, C. C., Meert, J. G., Pandit, M. K. & Kamenov, G. D., 2014. A detrital zircon U-Pb and Hf isotopic transect across the Son Valley sector of the Vindhyan basin, India: implications for basin evolution and paleogeography. *Gondwana Research*, 26(1), 348-364. https://doi.org/10.1016/j.gr.2013.07.009

Valley, J. W., Kinny, P. D., Schulze, D. J., & Spicuzza, M. J., 1998. Zircon megacrysts from kimberlite: oxygen isotope variability among mantle melts. *Contributions to mineralogy and petrology*, 133(1), 1-11. https://doi.org/10.1007/s004100050432

Verdel, C., Campbell, M. J., & Allen, C. M., 2021. Detrital zircon petrochronology of central Australia, and implications for the secular record of zircon trace element composition. *Geosphere*, 17(2), 538-560. https://doi.org/10.1130/GES02300.1

Wang Q. F., Deng J., Li, C.S., Li, G. J., Li, Y., Qiao, L., 2014. The boundary between the Simao and Yangtze blocks and their locations in Gondwana and Rodinia: Constraints from detrital and inherited zircons. *Gondwana Research*, 26(2):438-448. https://doi.org/10.1016/j.gr.2013.10.002

Wang, J. Q., Shu, L. S., & Santosh, M., 2017b. U-Pb and Lu-Hf isotopes of detrital zircon grains from Neoproterozoic sedimentary rocks in the central Jiangnan Orogen, South China: Implications for Precambrian crustal evolution. *Precambrian Research*, 294, 175-188. https://doi.org/10.1016/j.precamres.2017.03.025

Wang, J. Q., Shu, L. S., Santosh, M. & Xu, Z. Q., 2015. The pre-Mesozoic crustal evolution of the Cathaysia Block, South China: insights from geological investigation, zircon U-Pb geochronology, Hf isotope and REE geochemistry from the Wugongshan complex. *Gondwana Research*, 28(1), 225-245. DOI: 10.1016/j.gr.2014.03.008

Wang, J., & Li, Z. X., 2003. History of Neoproterozoic rift basins in South China:

implications for Rodinia break-up. *Precambrian Research*, 122(1-4), 141-158. https://doi.org/10.1016/S0301-9268(02)00209-7

Wang, K. X., Sun, L. Q., Sun, T., Huang, H., & Qin, L. S., 2018c. Provenance, weathering conditions, and tectonic evolution history of the Cambrian meta-sediments in the Zhuguangshan area, Cathaysia Block. *Precambrian Research*, 311, 195-210. https://doi.org/10.1016/j.precamres.2018.04.011

Wang, L. J., Yu, J. H., Griffin, W. L. & O'Reilly, S.Y., 2012a. Early crustal evolution in the western Yangtze block: evidence from U-Pb and Lu-Hf isotopes on detrital zircons from sedimentary rocks. *Precambrian Research*, 222-223, 368-385. https://doi.org/10.1016/j.precamres.2011.08.001

Wang, P. M., Yu, J. H., Sun, T., Ling, H. F., Chen, P. R., Zhao, K. D., Chen, W. F. & Liu, Q., 2012b. Geochemistry and detrital zircon geochronology of Neoproterozoic sedimentary rocks in eastern Hunan Province and their tectonic significance. *Acta Petrologica Sinica*, 28(12), 3841-3857. (in Chinese with English abstract)

Wang, P. M., Yu, J. H., Sun, T., Shi, Y., Chen, P. R., Zhao, K. D., Chen, W. F., & Liu, Q., 2013a. Composition variations of the Sinian-Cambrian sedimentary rocks in Hunan and Guangxi provinces and their tectonic significance. *Science China-Earth Sciences*, 56(11), 1899-1917. DOI: 10.1007/s11430-013-4634-1

Wang, W., Cawood, P. A., Pandit, M. K., Xia, X. P., Raveggi, M., Zhao, J. H., Zheng, J. P., & Qi, L., 2021. Fragmentation of South China from greater India during the Rodinia-Gondwana transition. *Geology*, 49(2), 228-232. DOI: 10.1130/G48308.1

Wang, W., Cawood, P. A., Pandit, M. K., Zhao, J. H., & Zheng, J. P., 2019a. No collision between Eastern and Western Gondwana at their northern extent. *Geology*, 47(4), 308-798. https://doi.org/10.1130/G45745.1

Wang, W., Cawood, P. A., Zhou, M. F., Pandit, M. K., Xia, X. P., & Zhao, J. H., 2017a. Low-delta O-18 Rhyolites from the Malani Igneous Suite: A Positive Test for South China and NW India Linkage in Rodinia. *Geophysical Research Letters*, 44(20), 10298-10305. DOI: 10.1002/2017GL074717

Wang, W., Zeng, M. F., Zhou, M. F., Zhao, J. H., Zheng, J. P., & Lan, Z. F., 2018b. Age, provenance and tectonic setting of Neoproterozoic to early Paleozoic

903 sequences in southeastern South China block: constraints onits linkage to western
904 Australia-east Antarctica. *Precambrian Research*, 309, 290-308.
905 https://doi.org/10.1016/j.precamres.2017.03.002
906 Wang, X. C., Li, X. H., Li, W. X., & Li, Z. X., 2007a. Ca. 825 Ma komatiitic basalts
907 in South China: First evidence for> 1500 $^{0}$C mantle melts by a Rodinian mantle
908 plume. *Geology*, 35(12), 1103-1106. https://doi.org/10.1130/G23878A.1
909 Wang, X. C., Li, X. H., Li, Z. X., Li, Q. L., Tang, G. Q., Gao, Y. Y., Zhang, Q. R., &
910 Liu, Y., 2012c. Episodic Precambrian crust growth: Evidence from U-Pb ages and
911 Hf-O isotopes of zircon in the Nanhua Basin, central South China. *Precambrian*
912 *Research*, 222, 386-403. DOI: 10.1016/j.precamres.2011.06.001
913 Wang, X. C., Li, Z. X., Li, X. H., Li, Q. L., Tang, G. Q., Zhang, Q. R., Liu, Y., 2011.
914 Nonglacial origin for low-delta O-18 Neoproterozoic magmas in the South China
915 Block: Evidence from new in-situ oxygen isotope analyses using SIMS. *Geology*,
916 39(8), 735-738. DOI: 10.1130/G31991.1
917 Wang, X. L., Zhou, J. C., Griffin, W. L. , Wang, R. C., Qiu, J. S., Reilly, S.Y. O., Xu,
918 X. S., Liu, X. M. & Zhang, G. L., 2007b. Detrital zircon geochronology of
919 Precambrian basement sequences in the Jiangnan Orogen: dating the assembly of
920 the Yangtze and Cathaysia Blocks. *Precambrian Research*, 159(1-2), 117-131.
921 https://doi.org/10.1016/j.precamres.2007.06.005
922 Wang, X. L., Zhou, J. C., Wan, Y. S., Kitajima, K., Wang, D., Bonamici, C., Qiu, J. S.
923 & Sun, T., 2013b. Magmatic evolution and crustal recycling for Neoproterozoic
924 strongly peraluminous granitoids from southern China: Hf and O isotopes in zircon.
925 *Earth and Planetary Science Letters*, 366, 71-82.
926 https://doi.org/10.1016/j.epsl.2013.02.011
927 Wang, Y. J., Zhang, F. F., Fan, W. M., Zhang, G. W., Chen, S. Y., Cawood, P. A.,
928 Zhang, A. M., 2010. Tectonic setting of the South China Block in the early
929 Paleozoic: Resolving intracontinental and ocean closure models from detrital zircon
930 U-Pb geochronology. *Tectonics*, 29(6), 1-16. DOI: 10.1029/2010TC002750
931 Wang, Z. H., Yang, W. Q., Zhou, D., Niu, Z. J., He, Y. Y., Song, F., 2018a. Detrital
932 Zircon U-Pb Geochronological Records and Its Response of Provenance

Transformation of Strata Surrounding Cambrian-Devonian Unconformity in Eastern Margin of Yunkai Massif. *Earth Science*, 43(11): 4193-4203. (in Chinese with English abstract). https:// doi.org/10.3799/dqkx.2018.242

Wu, L., Jia, D., Li, H. B., Deng, F. & Li, Y. Q., 2010. Provenance of detrital zircons from the Late Neoproterozoic to Ordovician sandstones of South China: implications for its continental affinity. *Geological Magazine*, 147(06), 974-980. DOI: 10.1017/S0016756810000725

Wu, P., Zhang, S. B., Zheng, Y. F., Li, Q. L., Li, Z. X., & Sun, F. Y., 2020. The occurrence of Neoproterozoic low delta O-18 igneous rocks in the northwestern margin of the South China Block: Implications for the Rodinia configuration. *Precambrian Research*, 347, 105841. DOI: 10.1016/j.precamres.2020.105841

Wu, Y. W., 2013. The evolution record of Longmuco-Shuanghu-Lancang Ocean-Cambrian-Permian ophiolites. (Doctoral dissertation). Changchun, Jilin: Jilin University. (in Chinese with English abstract).

Xiang, L. and Shu, L. S., 2010. Pre-Devonian tectonic evolution of the eastern South China Block: Geochronological evidence from detrital zircons. *Science China Earth Science*, 40(10): 1377-1388. (in Chinese with English abstract) DOI: 10.1007/s11430-010-4061-5

Xiong, C., Niu, Y. L., Chen, H. D., Chen, A. Q., Zhang, C. G., Li, F., Yang, S. & Xu, S. L., 2019. Detrital zircon U-Pb geochronology and geochemistry of late Neoproterozoic-early Cambrian sedimentary rocks in the Cathaysia block: constraint on its palaeo-position in Gondwana supercontinent. *Geological Magazine*, 156(9), 1587-1604. DOI: https://doi.org/10.1017/S0016756819000013

Xu, Y. J., Cawood, P. A., Du, Y. S., Hu, L. S., Yu, W. C., Zhu, Y. H., & Li, W. C., 2013. Linking South China to northern Australia and India on the margin of Gondwana: Constraints from detrital zircon U-Pb and Hf isotopes in Cambrian strata. *Tectonics*, 32(6), 1547-1558. https://doi.org/10.1002/tect.20099

Xu, Y. J., Cawood, P. A., Du, Y. S., Huang, H. W., & Wang, X. Y., 2014. Early Paleozoic orogenesis along Gondwana's northern margin constrained by provenance data from South China. *Tectonophysics*, 636, 40-51.

https://doi.org/10.1016/j.tecto.2014.08.022

Xue, E. K., Wang, W., Huang, S. F., & Lu, G. M., 2019. Detrital zircon U-Pb-Hf isotopes and whole-rock geochemistry of Neoproterozoic-Cambrian successions in the Cathaysia Block of South China: Implications on paleogeographic reconstruction in supercontinent. *Precambrian Research*, 331, 105348. https://doi.org/10.1016/j.precamres.2019.105348

Yan, C. L., Shu, L. S., Faure, M., Chen, Y., & Huang, R. B., 2019. Time constraints on the closure of the Paleo-South China Ocean and the Neoproterozoic assembly of the Yangtze and Cathaysia blocks: Insight from new detrital zircon analyses. *Gondwana Research*, 73, 175-189. https://doi.org/10.1016/j.gr.2019.03.018

Yan, C. L., Shu, L. S., Santosh, M., Yao, J. L., Li, J. Y., & Li, C., 2015. The Precambrian tectonic evolution of the western Jiangnan Orogen and western Cathaysia Block: Evidence from detrital zircon age spectra and geochemistry of clastic rocks. *Precambrian Research*, 268, 33-60. https://doi.org/10.1016/j.precamres.2015.07.002

Yang, C., Li, X. H., Wang, X. C., & Lan, Z., 2015. Mid-Neoproterozoic angular unconformity in the Yangtze Block revisited: insights from detrital zircon U-Pb age and Hf-O isotopes. *Precambrian Research*, 266, 165-178. https://doi.org/10.1016/j.precamres.2015.05.016

Yang, Y. N., Wang, X. C., Li, Q. L., & Li, X. H., 2016. Integrated in situ U-Pb age and Hf-O analyses of zircon from Suixian Group in northern Yangtze: New insights into the Neoproterozoic low-delta O-18 magmas in the South China Block. *Precambrian Research*, 273, 151-164. DOI: 10.1016/j.precamres.2015.12.008

Yang, Z. Y., & Jiang, S. Y., 2019. Detrital zircons in metasedimentary rocks of Mayuan and mamianshan group from Cathaysia block in northwestern Fujian province, South China: new constraints on their formation ages and paleogeographic implication. *Precambrian Research*, 320, 13-30. https://doi.org/10.1016/j.precamres.2018.10.004

Yang, Z. Y., Sun, Z. M., Yang, T. S., & Pei, J. L., 2004. A Long Connection (750-380 Ma) between South China and Australia: Paleomagnetic Constraints. *Earth and*

*Planetary Science Letters*, 220, 423-434. https://doi.org/10.1016/S0012-821X(04)00053-6

Yao, J. L., Cawood, P. A., Shu, L. S., & Zhao, G. C., 2019. Jiangnan Orogen, South China: A similar to 970-820 Ma Rodinia margin accretionary belt. *Earth Science Reviews*, 196, 102872. DOI: 10.1016/j.earscirev.2019.05.016

Yao, J. L., Shu, L. S. & Santosh, M., 2011. Detrital zircon U-Pb geochronology, Hf-isotopes and geochemistry-new clues for the Precambrian crustal evolution of Cathaysia block, South China. *Gondwana Research*, 20(2-3), 553-567. https://doi.org/10.1016/j.gr.2011.01.005

Yao, W. H., Li, Z. X., Li, W. X., Li, X. H., & Yang, J. H., 2014. From Rodinia to Gondwanaland: a tale of detrital zircon provenance analyses from the southern Nanhua basin, South China. *American Journal of Science*, 314(1), 278-313. DOI:10.2475/01.2014.08

Yao, W. H., Li, Z. X., Li, W. X., Su, L. & Yang, J. H., 2015. Detrital provenance evolution of the Ediacaran-Silurian Nanhua Foreland basin, South China. *Gondwana Research*, 2015, 28(4), 1449-1488. DOI: 10.1016/j.gr.2014.10.018

Yu, J. H., Reilly, S. Y. O, Wang, L. J., Griffin, W. L., Zhou, M. F., Zhang, M. & Shu, L. S., 2010. Components and episodic growth of Precambrian crust in the Cathaysia block, South China: evidence from U-Pb ages and Hf isotopes of zircons in Neoproterozoic sediments. *Precambrian Research*, 181(1-4), 97-114. https://doi.org/10.1016/j.precamres.2010.05.016

Yuan, H. Y., Zhou, Q., Ding, J., Zhang, H. H., Zhu, L. T., Liang, J., Tang, G. L., & Wang, C. N., 2017. U-Pb Geochronological Studies on Detrital Zircon in Jianglang Group，Western Sichuan Province，China. *Acta Mineralogical Sinica*, 37(3), 296-304. DOI: 10.1016/j.lithos.2021.106108 (in Chinese with English abstract)

Yuan, X. Y., Niu, M. L., Cai, Q. R., Wu, Q., Zhu, G., Li, X. C., Sun, Y., & Li, C., 2021. Bimodal volcanic rocks in the northeastern margin of the Yangtze Block: Response to breakup of Rodinia supercontinent. *Lithos*, 390, 106108. DOI: 10.1016/j.lithos.2021.106108

Zhang, H., Liu, Y. X., Ding, X. Z., Gao, L. Z., Yang, C., Zhang, J. B., Gong, C. Q. &

Liu, H. G., 2020a. Geochronology, Geochemistry, Whole Rock Sr-Nd and Zircon Hf-O Isotopes of the Early Neoproterozoic Volcanic Rocks in Jiangshan, Eastern Part of the Jiangnan Orogen: Constraints on Petrogenesis and Tectonic Implications. *Acta Geologica Sinica-English Edition*, 94(4), 1117-1137. DOI: 10.1111/1755-6724.14561

Zhang, J. B., Ni, J. B., Liu, Y. X., Zhang, H., & Bu, L., 2020b. Ordovician Proto-basin in South China and its Tectonic Implications: Evidence from the Detrital Zircon U-Pb Ages of the Ordovician in Central Hunan, China. *Acta Geologica Sinica-English Edition*, 94(6), 2115-2133. DOI:10.1111/1755-6724.14583

Zhang, J. W., Ye, T. P., Dai, Y. R., Chen, J. S., Zhang, H., Dai, C. G., Yuan, G. H. & Jiang, K. Y., 2019a. Provenance and tectonic setting transition as recorded in the Neoproterozoic strata, western Jiangnan Orogen: Implications for South China within Rodinia. *Geoscience Frontiers*, 10(5), 1823-1839. https://doi.org/10.1016/j.gsf.2018.10.009

Zhang, X. C., Wang, Y. J., Clift, P. D. Yan, Y., Zhang, Y. Z. & Zhang, L., 2018. Paleozoic Tectonic Setting and Paleogeographic Evolution of the Qin-Fang Region, Southern South China Block: Detrital Zircon U-Pb Geochronological and Hf Isotopic Constraints. *Geochemistry, Geophysics, Geosystems*, 19(10), 3962-3979. https://doi.org/10.1029/2018GC007713

Zhang, X. Z., Dong, Y. S., Li, C., Deng, M. R., Zhang, L. & Xu, W., 2014. Silurian high-pressure granulites from Central Qiangtang, Tibet: constraints on early Paleozoic collision along the northeastern margin of Gondwana. *Earth and Planetary Science Letters*, 405, 39-51. DOI: 10.1016/j.epsl.2014.08.013

Zhang, Y. L., Jia, X. T., Wang, Z. Q., Wang, K. M., Chen, M. Y., 2019b. Paleogeography and provenance analysis of Early Cambrian Xiannvdong Formation in the Micangshan area. *Acta Geologica Sinica*, 93(11): 2904-2920. DOI:10.19762/j.cnki.dizhixuebao.2019094. (in Chinese with English abstract)

Zhao, B. X., Long, X. P., Luo, J., Dong, Y. P., Lan, C. Y., Wang, J. Y. & Wu, B., 2021. Late Neoproterozoic to early Paleozoic paleogeographic position of the Yangtze block and the change of tectonic setting in its northwestern margin: Evidence from

detrital zircon U-Pb ages and Hf isotopes of sedimentary rocks. *GSA Bulletin*. https://doi.org/10.1130/B35980.1

Zhao, G. C. & Cawood, P. A., 1999. Tectonothermal evolution of the Mayuan Assemblage in the Cathaysia Block; implications for Neoproterozoic collision-related assembly of the South China Craton. *American Journal of Science*, 299 (4), 309-339. DOI: https://doi.org/10.2475/ajs.299.4.309

Zhao, G. C., Wang, Y. J., Huang, B. C., Dong, Y. P., Li, S. Z., Zhang, G. W. & Yu, S., 2018a. Geological reconstructions of the East Asian blocks: from the breakup of Rodinia to the assembly of Pangea. *Earth Science Reviews*, 186, 262-286. DOI: 10.1016/j.earscirev.2018.10.003

Zhao, J. H., Asimow, P. D., Zhou, M. F., Zhang, J., Yan, D. P., & Zheng, J. P., 2017. An Andean-type arc system in Rodinia constrained by the Neoproterozoic Shimian ophiolite in South China. *Precambrian Research*, 296, 93-111. https://doi.org/10.1016/j.precamres.2017.04.017

Zhao, J. H., Pandit, M. K., Wang, W., & Xia, X. P., 2018b. Neoproterozoic tectonothermal evolution of NW India: Evidence from geochemistry and geochronology of granitoids. *Lithos*, 316, 330-346. DOI:10.1016/j.lithos.2018.07.020

Zhao, J. H., Pandit, M. K., Wang, W., & Xia, X. P., 2018c. Neoproterozoic tectonothermal evolution of NW India: Evidence from geochemistry and geochronology of granitoids. *Lithos*, 316, 330-346. DOI:10.1016/j.lithos.2018.07.020

Zhao, J. H., Zhou, M. F., Yan, D. P., Yang, Y. H., & Sun, M., 2008. Zircon Lu-Hf isotopic constraints on Neoproterozoic subduction-related crustal growth along the western margin of the Yangtze Block, South China. *Precambrian Research*, 163(3-4), 189-209. https://doi.org/10.1016/j.precamres.2007.11.003

Zhao, J. H., Zhou, M. F., Yan, D. P., Zheng, J. P., & Li, J. W., 2011. Reappraisal of the ages of Neoproterozoic strata in South China: no connection with the Grenvillian orogeny. *Geology*, 39(4), 299-302. https://doi.org/10.1130/G31701.1

Zhao, J. H., Zhou, M. F., Zheng, J. P., & Fang, S. M., 2010. Neoproterozoic crustal

growth and reworking of the Northwestern Yangtze Block: constraints from the Xixiang dioritic intrusion, South China. *Lithos*, 120(3-4), 439-452. https://doi.org/10.1016/j.lithos.2010.09.005

Zhao, Z. B., Xu, Z. Q., Ma, X. X., Liang, F. H., & Guo, P., 2018d. Neoproterozoic-Early Paleozoic tectonic evolution of the South China Craton: New insights from the polyphase deformation in the southwestern Jiangnan orogen. *Acta Geologica Sinica-English Edition*, 92(5), 1700-1727. https://doi.org/10.1111/1755-6724.13672

Zhou, J. L., 2015b. Tectonic affinity of the Neoproterozoic-aged Imorona-Itsindro Suite in Masagascar and its geological significance. China University of Geosciences (Beijing). (in Chinese with English abstract).

Zhou, J. L., Li, X. H., & Tucker, R. D., 2020. New insights into the genesis of Neoproterozoic low-delta O-18 granitoids in the Seychelles: crustal cannibalization within an intra-plate extensional setting. *Science Bulletin*, 65(22), 1880-1883. DOI: 10.1016/j.scib.2020.07.025

Zhou, J. L., Li, X. H., Tang, G. Q., Liu, Y., & Tucker, R. D., 2017. New evidence for a continental rift tectonic setting of the Neoproterozoic Imorona-Itsindro Suite (central Madagascar). *Precambrian Research*, 306, 94-111. DOI: 10.1016/j.precamres.2017.12.029

Zhou, J. L., Li, X. H., Tang, G. Q., Liu, Y., & Tucker, R. D., 2018a. New evidence for a continental rift tectonic setting of the Neoproterozoic Imorona-Itsindro Suite (central Madagascar). *Precambrian Research*, 306, 94-111. DOI: 10.1016/j.precamres.2017.12.029

Zhou, J. L., Shao, S., Luo, Z. H., Shao, J. B., Wu, D. T., & Rasoamalala, V., 2015a. Geochronology and geochemistry of Cryogenian gabbros from the Ambatondrazaka area, east-central Madagascar: Implications for Madagascar-India correlation and Rodinia paleogeography. *Precambrian Research*, 256, 256-270.https://doi.org/10.1016/j.precamres.2014.11.005

Zhou, M. F., Ma, Y., Yan, D. P., Xia, X., Zhao, J. H., & Sun, M., 2006. The Yanbian terrane (Southern Sichuan Province, SW China): a Neoproterozoic arc assemblage

in the western margin of the Yangtze block. *Precambrian Research*, 144(1-2), 19-38. https://doi.org/10.1016/j.precamres.2005.11.002

Zhou, X. Y., Yu, J. H., O'Reilly, S. Y., Griffin, W. L., Sun, T., Wang, X. L., Tran, M. D. & Nguyen, D. L., 2018b. Component variation in the late Neoproterozoic to Cambrian sedimentary rocks of SW China-NE Vietnam, and its tectonic significance. *Precambrian Research*, 308, 92-110. DOI:10.1016/j.precamres.2018.02.003

Zhu, D. C., Zhao, Z. D., Niu, Y. L., Dilek, Y., Wang, L. Q., & Mo, X. X., 2011. Lhasa terrane in Southern Tibet came from Australia. *Geology*, 39(8), 727-730. DOI: 10.1130/G31895.1

Zhu, G. L., Yu, J. H., Zhou, X. Y., Wang, X. L., & Wang, Y. D., 2019d. The western boundary between the Yangtze and Cathaysia blocks, new constraints from the Pingbian Group sediments, southwest South China Block. *Precambrian Research*, 331, 105350. https://doi.org/10.1016/j.precamres.2019.105350

Zhu, Y., Lai, S. C., Qin, J. F., Zhu, R. Z., Zhang, F. Y., Zhang, Z. Z, & Zhao, S. W., 2019a. Neoproterozoic peraluminous granites in the western margin of the Yangtze Block, South China: Implications for the reworking of mature continental crust. *Precambrian Research*, 333, 105443. DOI: 10.1016/j.precamres.2019.105443

Zou, H., Bagas, L., Li, X. Y., Liu, H., Jiang, X. W. & Li, Y., 2020. Origin and evolution of the Neoproterozoic Dengganping Granitic Complex in the western margin of the Yangtze Block, SW China: Implications for breakup of Rodina Supercontinent. *Lithos*, 370-371, 1-21. DOI: 10.1016/j.lithos.2020.105602

# Captions

**Table 1.** Location and stratigraphic information of samples analyzed

**Figure 1.** Simplified geological maps of (a) the Tibetan Plateau (after Tian et al., 2020), (b) the Yidun Terrane (after Peng et al., 2014), (c) the Gongling region of the Eastern Yidun subterrane (after BGMRSP, 1980, 1984) and (d) the Cryogenian-Ordovician strata and samples in the Gongling region (after BGMRSP, 1980, 1984). Abbreviations: ADFB, Aravalli-Delhi fold belt; CITZ, Central Indian tectonic zone; EGB, East Ghats belt; EYD, Eastern Yidun subterrane; WYD, Western Yidun subterrane.

**Figure 2.** Photographs of the representative (meta-)sedimentary samples from the Eastern Yidun subterrane. (a and b) the schist samples, (c) the sandstone sample, and (d) the slate sample. Abbreviations: Qtz, quartz; Pl, plagioclase; Mca, mica.

**Figure 3.** Concordia and detrital zircon age histogram-probability density distribution diagrams of the Neoproterozoic-Ordovician samples from the Eastern Yidun subterrane.

**Figure 4.** Plots of zircon $\varepsilon_{Hf}(t)$ versus U-Pb age of the Neoproterozoic (a) and Ordovician (b) detrital sediments in the Eastern Yidun subterrane. The detrital zircons $\varepsilon_{Hf}(t)$ data from the Yidun terrane (this study and Tian et al., 2020). The igneous zircons $\varepsilon_{Hf}(t)$ values of the Panxi-Hannan arc (data sources: Ao et al., 2019; Li et al., 2018; Qi & Zhao, 2020; Zhao et al., 2008a, 2010, 2017; Zhao et al., 2008b; Zhu et al., 2019a); The igneous zircons $\varepsilon_{Hf}(t)$ values of the Jiangnan Orogen

(data sources: Yao et al., 2019, and references therein).

**Figure 5.** Detrital zircon age distributions for late Tonian to Ordovician rocks from Yidun, South China, India and Australia terranes. Compilation of zircon age distribution of Neoproterozoic-Early Paleozoic sedimentary rocks from (A1-3) the Yidun terrane (This study and Tian et al., 2020), (B1-5) western Yangtze terrane (This study and Chen et al., 2016, 2018, 2021; Han et al., 2017; Hofmann et al., 2016; Liu et al., 2019c; Liu et al., 2020b; Luo et al., 2020; Sun et al., 2008, 2009; Tian et al., 2020; Wang et al., 2012a; Wang et al., 2014; Xia et al., 2016; Yuan et al., 2017; Zhang et al., 2019b; Zhao et al., 2021), (C1-5) the Nanhua basin (Cui et al., 2015; He et al., 2020; Liu et al., 2019a; Liu et al., 2019b; Ma et al., 2019; Sun et al., 2018; Qi et al., 2018; Wang et al., 2012b, 2013a; Wang et al., 2007b; Wang et al., 2017b; Wang et al., 2018a; Yan et al., 2019; Yang et al., 2015; Zhang et al., 2019a; Zhang et al., 2020b; Zhao et al., 2018c; Zhou et al., 2018b; Zhu et al., 2019b), (D1-5) the Cathaysia terrane (Qi et al., 2018, 2020; Wang et al., 2010; Wang et al., 2012b; Wang et al., 2015; Wang et al., 2018a; Wang et al., 2018b; Wang et al., 2018c; Wu et al., 2010; Xiang & Shu, 2010; Xiong et al., 2019; Xu et al., 2013, 2014; Xue et al., 2019; Yan et al., 2015; Yang & Jiang, 2019; Yao et al., 2011; Yao et al., 2014, 2015; Yu et al., 2010; Zhang et al., 2018; Zhou et al., 2018b), (E1-3) the western India terrane (Hughes et al., 2019; Lan et al., 2020; Malone et al., 2008; McKenzie et al., 2013; Myrow et al., 2010; Qasim et al., 2018; Turner et al., 2014; Wang et al., 2019a), (F1-5) the Aravalli-Delhi basin (DeCelles et al., 2000; Gehrels et al., 2006; Hofmann et al., 2011; Malone et al., 2008; Mukherjee et al., 2019; Myrow et al., 2010), (G1-5) the eastern India terrane (DeCelles et al., 2000; Gehrels et al., 2006, 2011; Hughes et al., 2011; Lan et al., 2020; Long et al., 2010; Malone et al., 2008; Mckenzie et al., 2011;

McQuarrie et al., 2013; Myrow et al., 2010; Turner et al., 2014), (H1-5) the Australia terrane (Haines et al., 2016; Johnson et al., 2016; Keemana et al., 2020; Mulder et al., 2020; Verdel et al., 2021).

**Figure 6.** Proposed tectonic framework and palaeogeographic position for South China, India, Seychelles and Madagascar in Rodinia during the Neoproterozoic (after Cawood et al., 2018; ; Wang et al., 2017a, 2021; Zhao et al., 2018b). Abbreviation: YD, Yidun Terrane. The Neoproterozoic igneous zircons $\varepsilon_{Hf}(t)$ and $\delta^{18}O$ data of the Madagascar terrane from (Armistead et al., 2019; Zhou et al., 2015, 2017); of the Seychelles terrane from (Harris & Ashwal, 2002; Shellnutt et al., 2020; Zhou et al., 2020); of the NW India from (Wang et al., 2017a); of the western Yangzte terrane from (Jiang et al., 2020; Qi & Zhao, 2020; Wu et al., 2020; Yang et al., 2016; Zou et al., 2020); of the Aravalli-Nanhua rift basin from (Huang et al., 2018; Wang et al., 2011, 2012c; Yuan et al., 2021; Zhao et al., 2018b).

**Figure 7.** Depositional setting of the Cryogenian Qiasi Group in the Eastern Yidun subterrane as inferred by discrimination plot of cumulative proportions vs. CA-DA of analyzed detrital zircons (after Cawood et al., 2012). Data are compiled from this study and Tian et al. (2020).

**Figure 8.** Tentative tectonic reconstruction models of South China (including the Yidun Terrane) along with other ambient terranes in Gondwana during Late Ediacaran-Early Cambrian (A) and Middle Cambrian-Early Ordovician (B) times (after Zhao et al., 2018a). Abbreviations: SC, South China; NC, North China.

**Figure 1.**

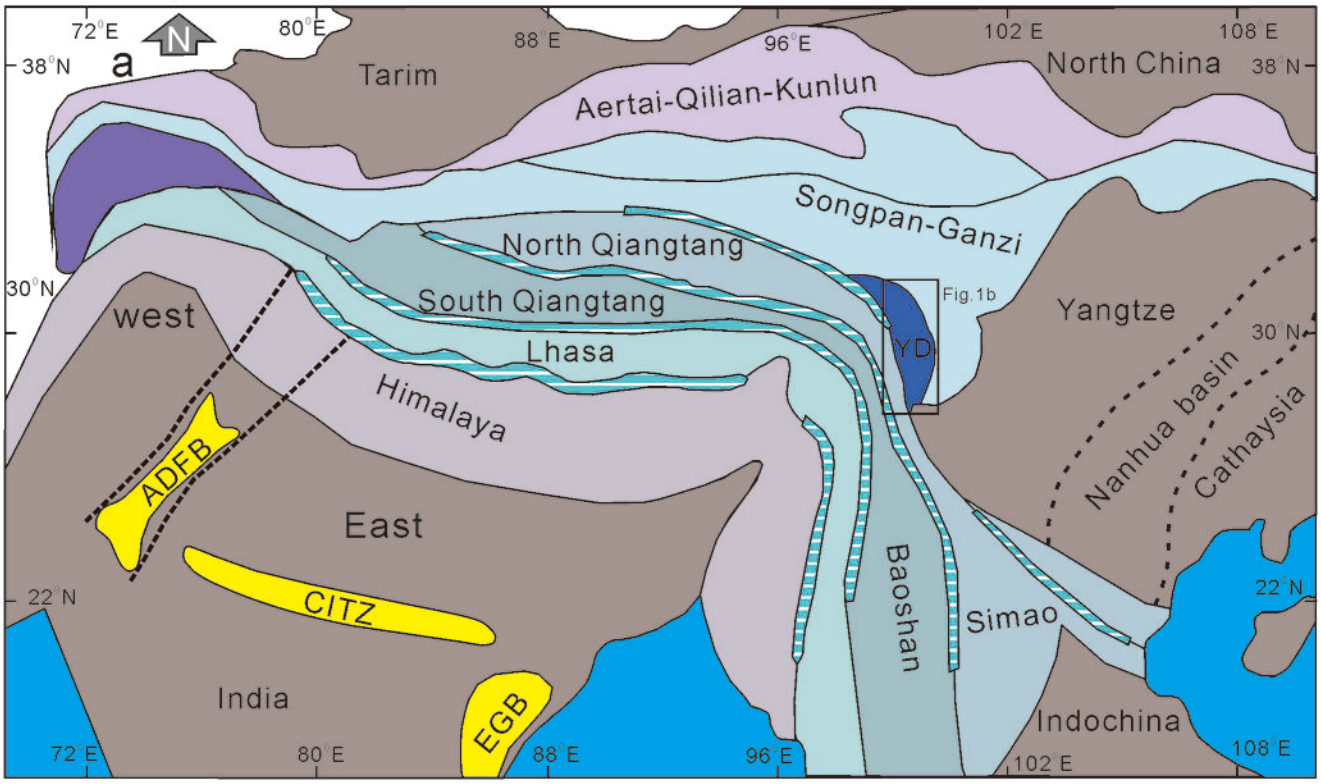


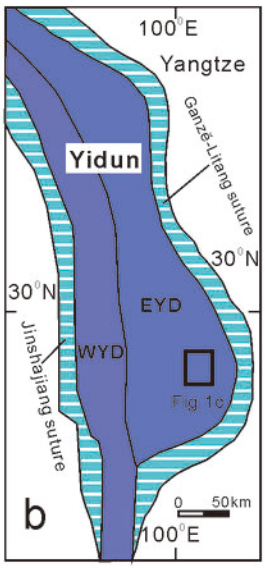


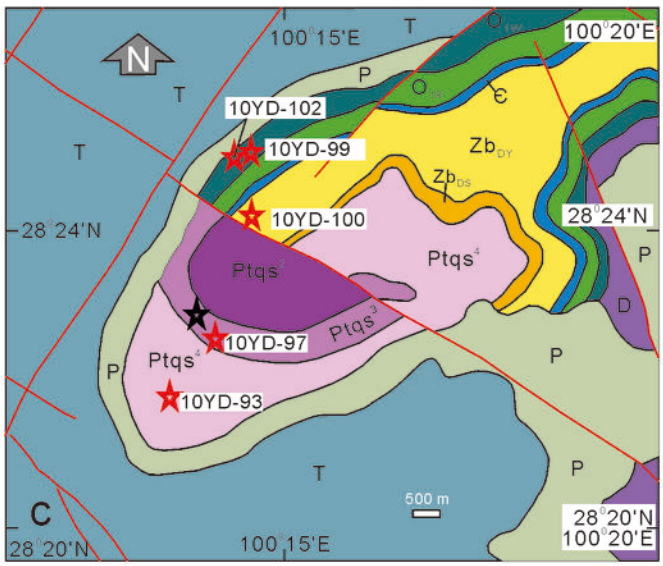


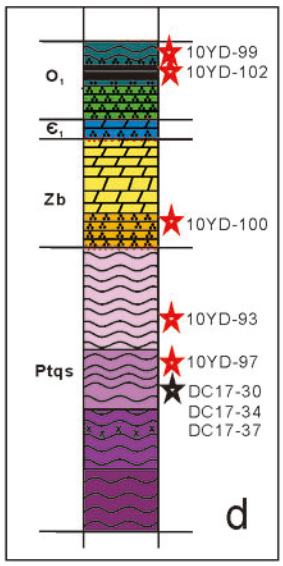


Ptqs⁴ Fourth member of Qiasi Group
Zb_DY Dengying Formation (Ediacaran)
Є Cambrian
Suture zone
Sandstone
This study
Ptqs³ Third member of Qiasi Group
Zb_DS Doushantou Formation (Ediacaran)
T Triassic
Dolomite
Slate
Literature samples
Ptqs² Second member of Qiasi Group
O_1W Wachang Formation (Ordovician)
D Devonian
Schist
Meta-diabase
Disconformity
Ptqs¹ First member of Qiasi Group
O_1R Rengong Formation (Ordovician)
P Permian
Siltstone
Fault
Unconformity

**Figure 2.**

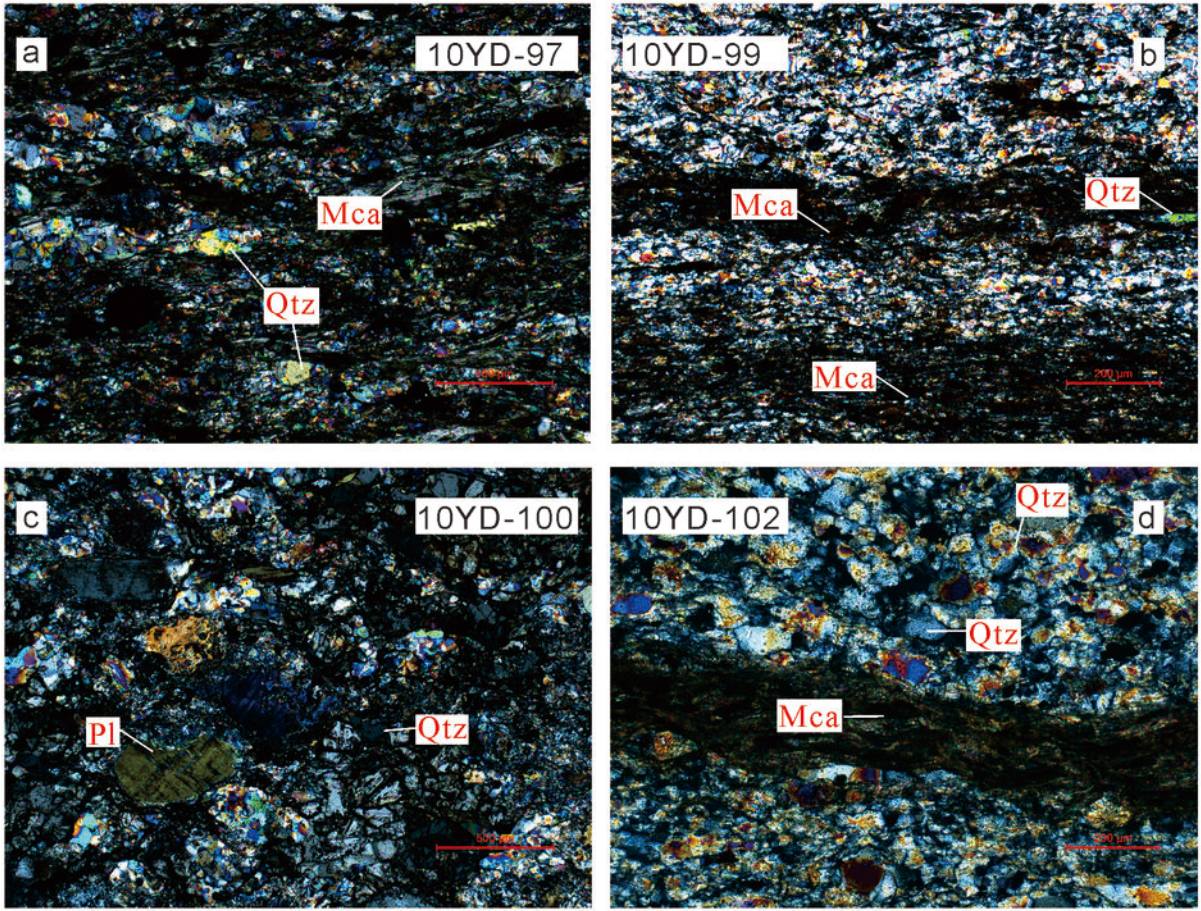
a
10YD-97
Mca
Qtz
10YD-99
b
Mca
Qtz
Mca
200 μm
c
10YD-100
Pl
Qtz
10YD-102
Qtz
d
Qtz
Mca

**Figure 3.**

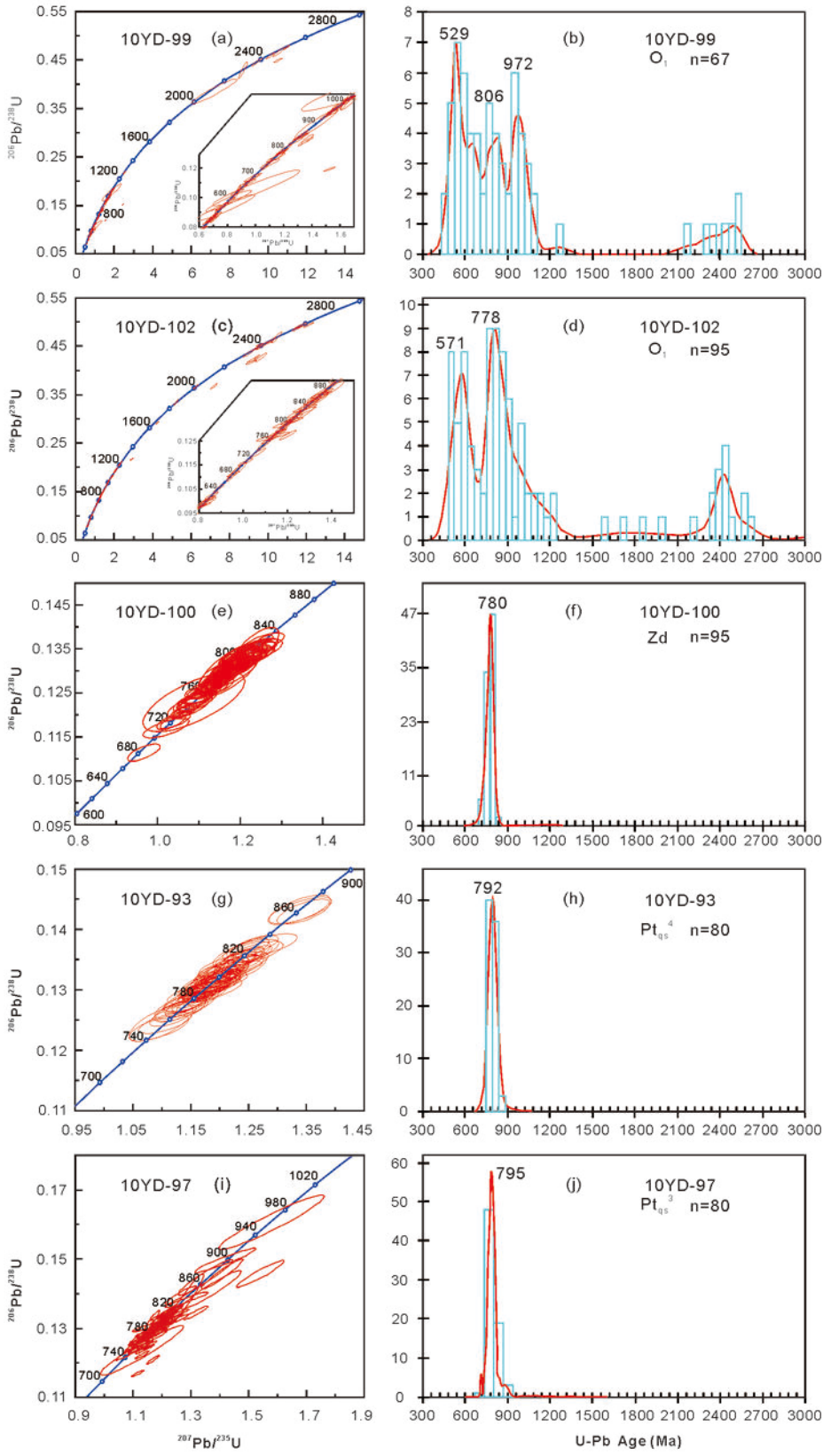
10YD-99 (a)
(b) 10YD-99
O1 n=67
529
972
806
10YD-102 (c)
(d) 10YD-102
O1 n=95
571
778
10YD-100 (e)
(f) 10YD-100
Zd n=95
780
10YD-93 (g)
(h) 10YD-93
Pt$_{qs}^{4}$ n=80
792
10YD-97 (i)
(j) 10YD-97
Pt$_{qs}^{3}$ n=80
795
$^{206}Pb/^{238}U$
$^{207}Pb/^{235}U$
U-Pb Age (Ma)

**Figure 4.**

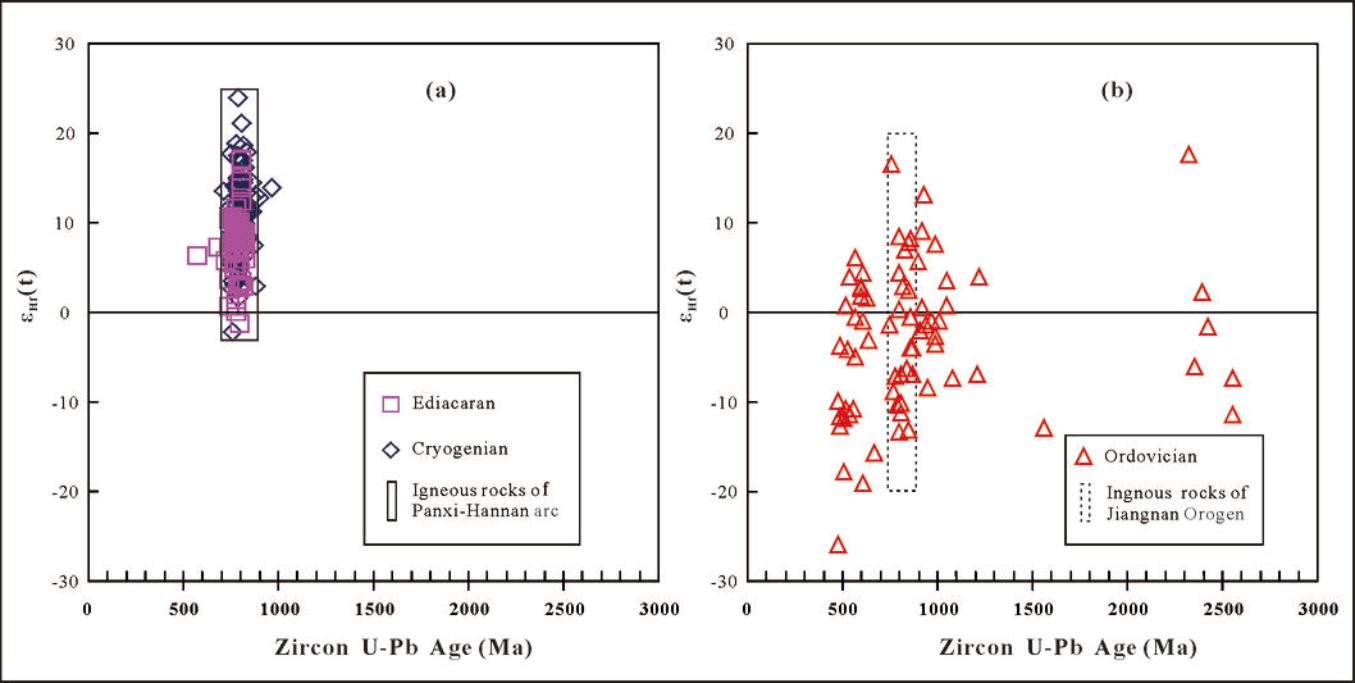
(a)
(b)
$\varepsilon_{Hf}(t)$
30
20
10
0
-10
-20
-30
0
500
1000
1500
2000
2500
3000
Zircon U-Pb Age (Ma)
Ediacaran
Cryogenian
Igneous rocks of Panxi-Hannan arc
Ordovician
Ingnous rocks of Jiangnan Orogen

**Figure 5.**

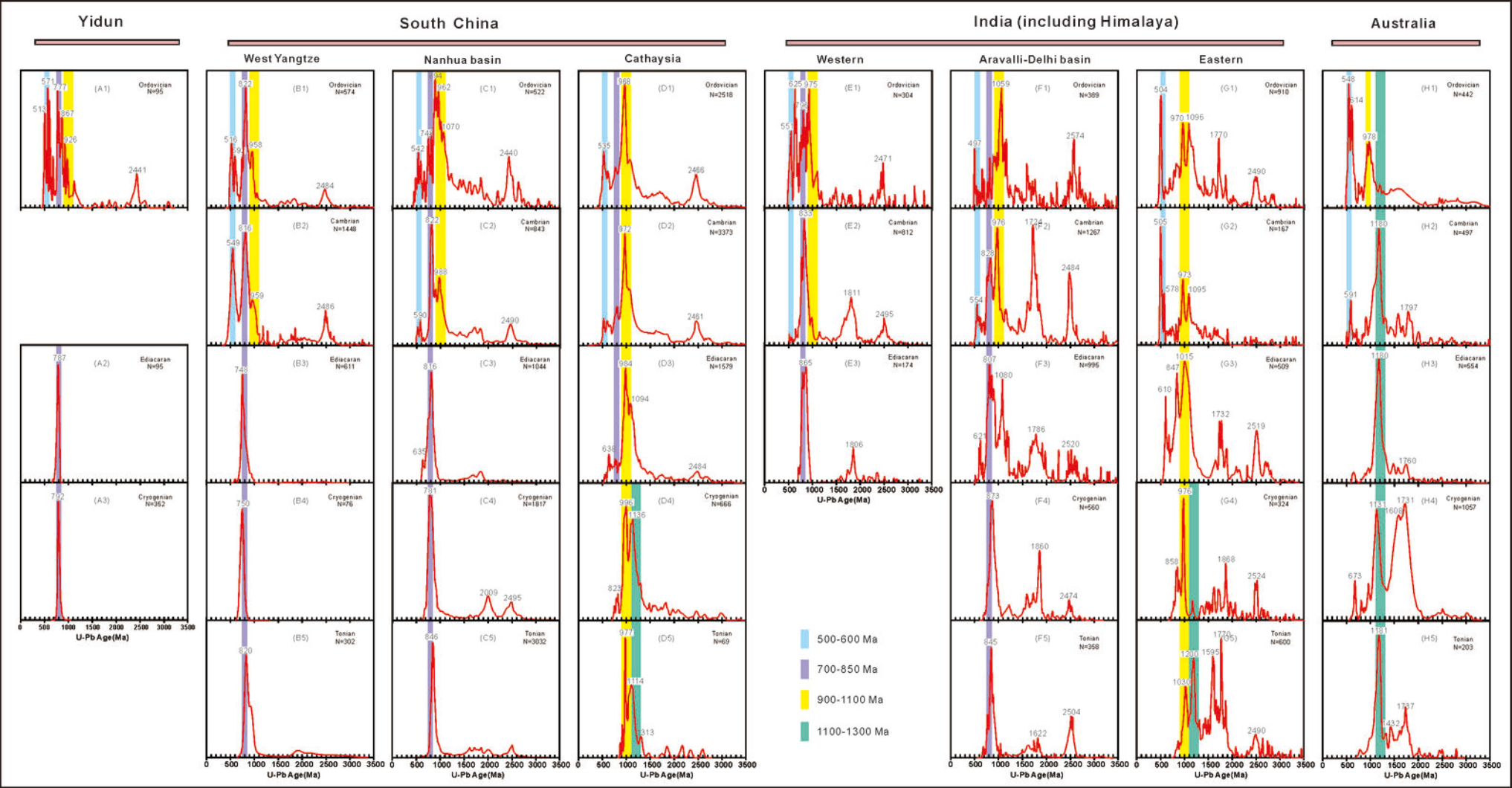
Yidun
South China
India (including Himalaya)
Australia
West Yangtze
Nanhua basin
Cathaysia
Western
Aravalli-Delhi basin
Eastern
(A1) Ordovician N=95
(A2) Ediacaran N=95
(A3) Cryogenian N=352
(B1) Ordovician N=574
(B2) Cambrian N=1448
(B3) Ediacaran N=611
(B4) Cryogenian N=76
(B5) Tonian N=302
(C1) Ordovician N=522
(C2) Cambrian N=843
(C3) Ediacaran N=1044
(C4) Cryogenian N=1817
(C5) Tonian N=3032
(D1) Ordovician N=2518
(D2) Cambrian N=3373
(D3) Ediacaran N=1579
(D4) Cryogenian N=666
(D5) Tonian N=69
(E1) Ordovician N=304
(E2) Cambrian N=812
(E3) Ediacaran N=174
(F1) Ordovician N=389
(F2) Cambrian N=1267
(F3) Ediacaran N=995
(F4) Cryogenian N=560
(F5) Tonian N=358
(G1) Ordovician N=910
(G2) Cambrian N=167
(G3) Ediacaran N=509
(G4) Cryogenian N=324
(G5) Tonian N=600
(H1) Ordovician N=442
(H2) Cambrian N=497
(H3) Ediacaran N=554
(H4) Cryogenian N=1057
(H5) Tonian N=203
U-Pb Age(Ma)
500-600 Ma
700-850 Ma
900-1100 Ma
1100-1300 Ma

**Figure 6.**

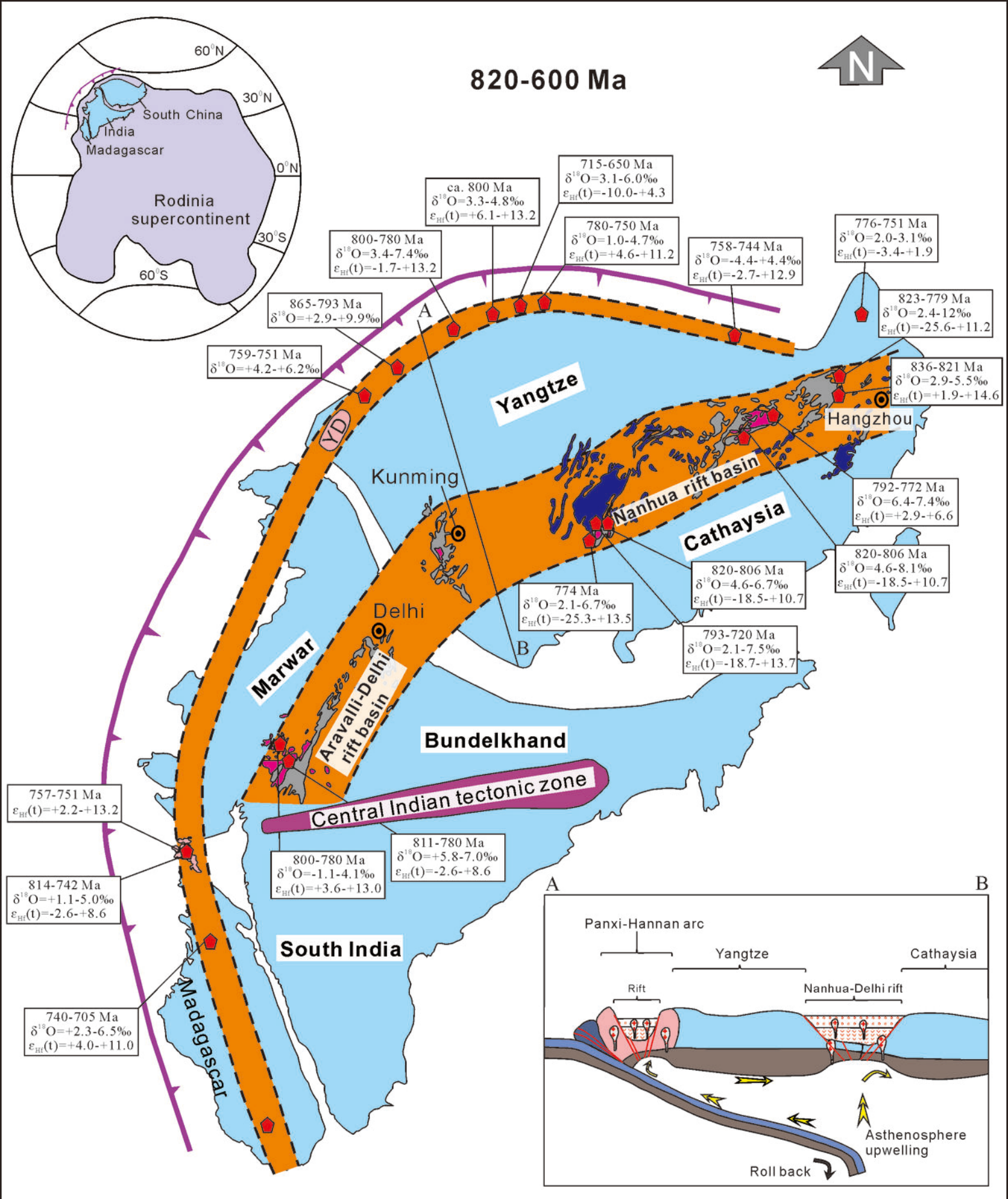
820-600 Ma
N
60°N
30°N
0°N
30°S
60°S
South China
India
Madagascar
Rodinia supercontinent
715-650 Ma
δ18O=3.1-6.0‰
εHf(t)=-10.0-+4.3
ca. 800 Ma
δ18O=3.3-4.8‰
εHf(t)=+6.1-+13.2
780-750 Ma
δ18O=1.0-4.7‰
εHf(t)=+4.6-+11.2
800-780 Ma
δ18O=3.4-7.4‰
εHf(t)=-1.7-+13.2
758-744 Ma
δ18O=-4.4-+4.4‰
εHf(t)=-2.7-+12.9
776-751 Ma
δ18O=2.0-3.1‰
εHf(t)=-3.4-+1.9
865-793 Ma
δ18O=+2.9-+9.9‰
823-779 Ma
δ18O=2.4-12‰
εHf(t)=-25.6-+11.2
759-751 Ma
δ18O=+4.2-+6.2‰
836-821 Ma
δ18O=2.9-5.5‰
εHf(t)=+1.9-+14.6
A
B
YD
Yangtze
Hangzhou
Kunming
Nanhua rift basin
Cathaysia
792-772 Ma
δ18O=6.4-7.4‰
εHf(t)=+2.9-+6.6
820-806 Ma
δ18O=4.6-8.1‰
εHf(t)=-18.5-+10.7
820-806 Ma
δ18O=4.6-6.7‰
εHf(t)=-18.5-+10.7
774 Ma
δ18O=2.1-6.7‰
εHf(t)=-25.3-+13.5
793-720 Ma
δ18O=2.1-7.5‰
εHf(t)=-18.7-+13.7
Delhi
Marwar
Aravalli-Delhi rift basin
Bundelkhand
Central Indian tectonic zone
757-751 Ma
εHf(t)=+2.2-+13.2
811-780 Ma
δ18O=+5.8-7.0‰
εHf(t)=-2.6-+8.6
800-780 Ma
δ18O=-1.1-4.1‰
εHf(t)=+3.6-+13.0
814-742 Ma
δ18O=+1.1-5.0‰
εHf(t)=-2.6-+8.6
South India
Madagascar
740-705 Ma
δ18O=+2.3-6.5‰
εHf(t)=+4.0-+11.0
A
B
Panxi-Hannan arc
Yangtze
Cathaysia
Rift
Nanhua-Delhi rift
Asthenosphere upwelling
Roll back
Meso- to Neoproterozoic strata
Neoproterozoic strata
Neoproterozoic (1.00-0.82 Ga) granitoids
Neoproterozoic subduct-related zone
Neoproterozoic rift-related basin
Late Neoproterozoic rift-related strata
A-type granite
Inferred subduction
Neoproterozoic low-δ18O igneous rocks

**Figure 7.**

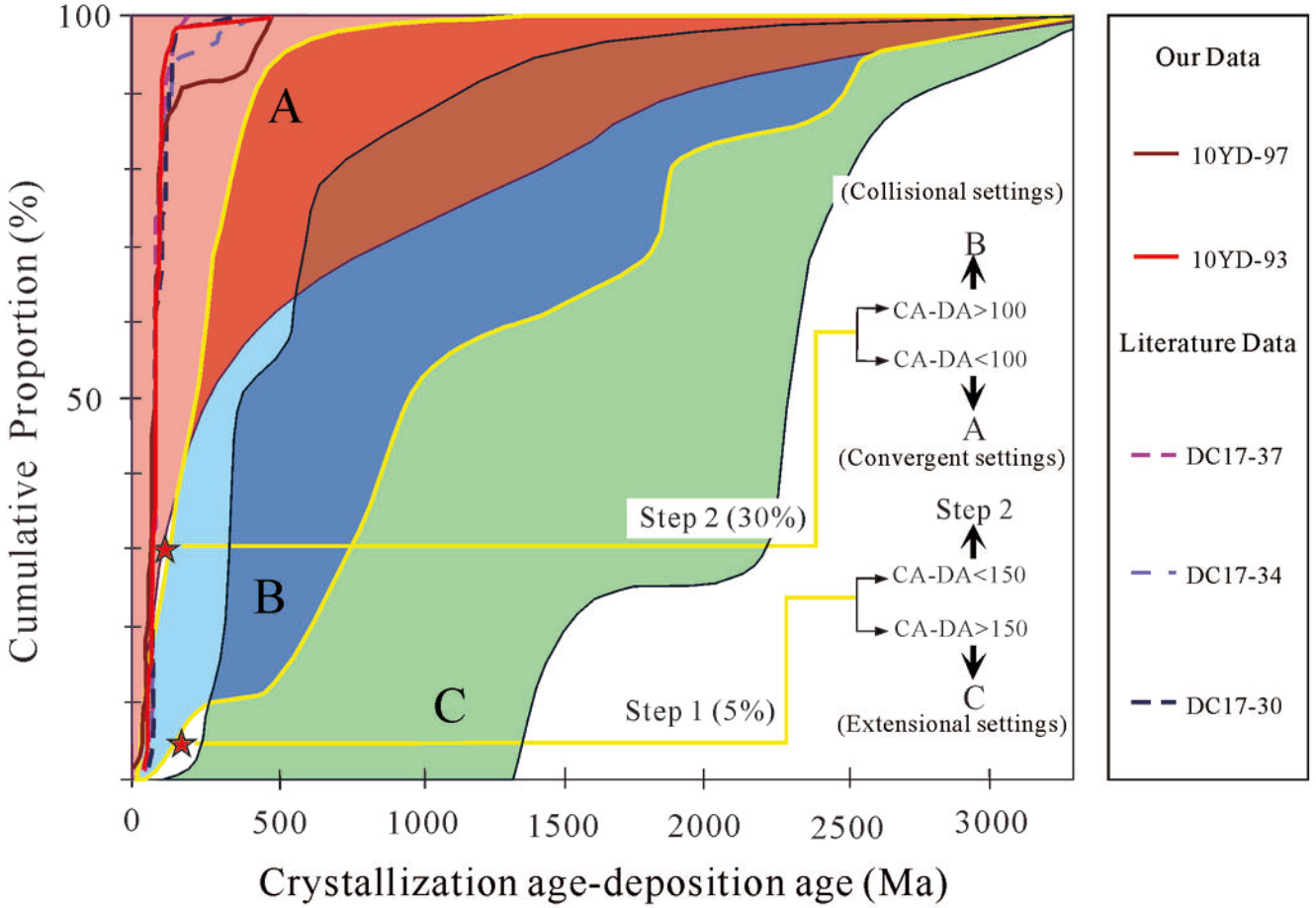
100
50
Cumulative Proportion (%)
A
B
C
(Collisional settings)
B
CA-DA>100
CA-DA<100
A
(Convergent settings)
Step 2 (30%)
Step 2
CA-DA<150
CA-DA>150
C
(Extensional settings)
Step 1 (5%)
0
500
1000
1500
2000
2500
3000
Crystallization age-deposition age (Ma)
Our Data
10YD-97
10YD-93
Literature Data
DC17-37
DC17-34
DC17-30

**Figure 8.**

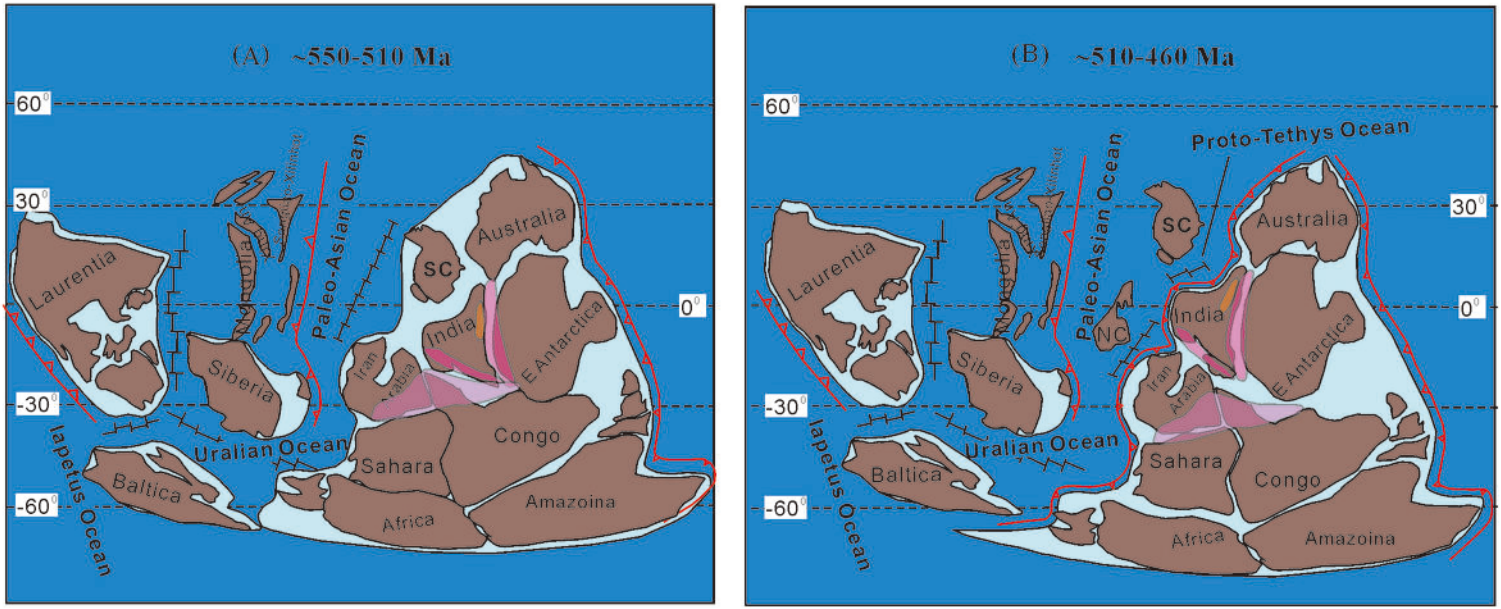
(A) ~550-510 Ma
60°
30°
0°
-30°
-60°
Laurentia
Mongolia
Kazakhstan
Paleo-Asian Ocean
Siberia
Uralian Ocean
Iapetus Ocean
Baltica
SC
Australia
India
Iran
Arabia
E.Antarctica
Congo
Sahara
Africa
Amazoina
(B) ~510-460 Ma
Proto-Tethys Ocean
NC
East African Orogen
Kuunga/Malagasy Orogen
East Ghat Belt
Ocean Spreading ridge
Subducted zone

Table 1.Location and stratigraphic information of samples analyzed

| Samples | Lithology | Latitude (N), Longitude (E) | Stratigraphic age | Mineral composition | Petrographical descriptions |
|---|---|---|---|---|---|
| 10YD-93 | Schist | N28°21.655, E100°13.619 | The fourth member of Qiasi Group ($Ptq^4$; Cryogenian) | Quartz (80-85%), mica (5-10%), lithic fragment (1-5%) and minor heavy minerals | Fine-grained, subangular to subrounded, moderately to well sorted, grain-supported, moderately texture maturity |
| 10YD-97 | Schist | N28°22.453, E100°14.064 | The third member of Qiasi Group ($Ptq^3$; Cryogenian) | Quartz (40-50%), mica (35-40%) and minor heavy minerals | Fine-grained, subangular to subrounded, moderately sorted, grain-supported, moderately texture maturity |
| 10YD-99 | Schist | N28°23.193, E100°14.410 | Wachang Fm. ($O_1$) | Quartz (60-65%), mica (20-35%), and minor heavy minerals | Fine-grained, subangular to subrounded, moderately to well sorted, grain-supported, moderately texture maturity |
| 10YD-100 | Sandstone | N28°24.153, E100°14.546 | Dengying Fm. (Ediacaran) | Quartz (70-80%), feldspar (10-15%) and minor heavy minerals | Middle- and fine-grained, angular to subangular, moderately to poorly sorted, grain-supported, moderately to low texture maturity |
| 10YD-102 | Slate | N28°24.958, E100°14.405 | Wachang Fm. ($O_1$) | Quartz (ca.70%), mica (20-25%), and minor heavy minerals | Fine-grained, subangular to subrounded, moderately sorted, matrix-supported, moderately texture maturity |